Evaluation of Traffic Speed Deflectometer for Collecting Network-Level Pavement Structural Data in Tennessee

Research Final Report from University of Tennessee, Knoxville | Baoshan Huang, Miaomiao Zhang, Hongren Gong, Pawel Polaczyk | May 30, 2022

Sponsored by Tennessee Department of Transportation Long Range Planning Research Office & Federal Highway Administration

DISCLAIMER

This research was funded through the State Planning and Research (SPR) Program by the Tennessee Department of Transportation and the Federal Highway Administration under ***RES 2020-08: Research Project Title: Evaluation of Traffic Speed Deflectometer for Collecting Network-Level Pavement Structural Data in Tennessee.***

Technical Report Documentation Page

1. Report No. RES2020-08	2. Government Accession No.	3. Recipient's Catalog No.
4. Title and Subtitle *Evaluation of Traffic Speed Deflectometer for Collecting Network-Level Pavement Structural Data in Tennessee*		5. Report Date May 2022 6. Performing Organization Code
7. Author(s) Baoshan Huang, Miaomiao Zhang, Hongren Gong, Pawel Polaczyk		8. Performing Organization Report No.
9. Performing Organization Name and Address The University of Tennessee, Knoxville Department of Civil and Environmental Engineering 851 Neyland Drive, 325 John D. Tickle Building Knoxville, TN 37996		10. Work Unit No. (TRAIS) 11. Contract or Grant No. RES2020-08
12. Sponsoring Agency Name and Address Tennessee Department of Transportation 505 Deaderick Street, Suite 900 Nashville, TN 37243		13. Type of Report and Period Covered Final Report July 2019 – May 2022 14. Sponsoring Agency Code
15. Supplementary Notes Conducted in cooperation with the U.S. Department of Transportation, Federal Highway Administration.		

16. Abstract

The Traffic Speed Deflectometer (TSD) overcomes the Falling Weight Deflectometer (FWD) limitations in terms of traffic interruption and testing inefficiency, which has been used for network-level pavement structural evaluation. However, some challenges exist as applying the TSD for routine survey works. A comparison of pavement response under the TSD and FWD is required to verify the applicability and substitutability of the TSD. In addition, the accuracy and precision of TSD measurements can be affected by several internal and external factors. This research project investigated the effect of load magnitude, test temperature, and test speed on TSD deflections, and a practical guideline for TSD data correction was provided. A new approach to determine the effective SN with TSD measurements was developed by modifying the AASHTO method. The possibility of estimating pavement fatigue conditions from TSD deflection lag was also evaluated. Results showed that the TSD deflection could be used to identify not only structurally weak sections, but also structurally weak layers. The loading frequency of the TSD is lower than that of the FWD, and the AC layer exhibits lower stiffness under the TSD. The lag distance increases with increasing fatigue levels. For the same road section (with the same pavement structure), the lag distance can indicate the initiation and growth of fatigue cracks in pavements.

17. Key Words **TSD, FWD, PMS, structure number, dynamic modulus, phase angle, lag**	18. Distribution Statement No restriction. This document is available to the public from the sponsoring agency at the website http://www.tn.gov/.

19. Security Classif. (of this report) Unclassified	20. Security Classif. (of this page) Unclassified	21. No. of Pages 71	22. Price

Acknowledgement

We would like to begin by thanking the Tennessee Department of Transportation (TDOT) for funding this research project. We have continued to collaborate closely with regional engineers and local technicians at the TDOT Materials and Test Division and local asphalt plants. They have provided valuable support towards the fulfillment of the research objectives. Without their support, it would be impossible for us to finish this research project. We would also like to thank the administrative staff from the TDOT Research Office who have worked very closely with our research team and kept the whole project on the proposed schedule.

Executive Summary

The incompleteness of construction history and the resulting inaccurate estimates of pavement structural capacity necessitates the use of innovative techniques to obtain accurate network-level pavement structural data for Tennessee. Currently, deflection measurements remain the only reliable non-destructive method for determining the structural strength of flexible pavements. The stationary Falling Weight Deflectometer (FWD) is the most prevailing method of deflection measurement. However, FWD is the preferred device for project-level structural evaluation, but issues such as time, expenses, and traffic control hinder FWD testing at the network-level. Recent technological advancements have led to the development of continuous deflection measurement devices, including the traffic speed deflectometer (TSD), to overcome the limitations of FWD.

Unlike static measurement devices, a TSD is capable of performing deflection surveys at traffic speeds, which provides a safe and efficient tool for collecting network-level pavement structural data. Since the TSD is a relatively new device, it is imperative to compare it with the existing measurement devices to validate its applicability and reliability [1]. In this research project, a total of 959 miles of TSD data were collected throughout Tennessee. Approximately 80 miles of these TSD routes were overlapped to verify the repeatability of the TSD deflection data. FWD testing was conducted at 190 test sites, and FWD measurements were compared to the corresponding TSD measurements. In addition, the rank correlation analysis was performed on TSD measurements and pavement performance data. The purpose of these comparisons is to incorporate TSD structural data into the pavement management system (PMS) to predict pavement conditions and select pavement maintenance and rehabilitation treatments more accurately.

TSDs can provide better spatial coverage and efficiency than FWDs. However, some challenges exist in applying a TSD for routine survey works. Several internal and external factors can influence the accuracy and precision of TSD measurements. Therefore, it is necessary to develop a reliable TSD deflection correction procedure so that TSD deflections collected at different trips or under different conditions will be comparable. This research project investigated the effect of load magnitude, test temperature, and test speed on TSD deflections, and a practical guideline for TSD data correction and analysis was provided.

In addition, a new approach to determine the effective structure number (SN) with TSD measurements was developed by modifying the AASHTO method so that the improved TSD-based SN can be comparable to the existing FWD-based SN records.

The viscoelasticity of the asphalt layer and the inertial damping of the structure may lead to a lag between the time when the TSD tire crosses the point and the time when the maximum response occurs. Therefore, there is a lag between the loading point and the point of maximum deflection in the basin, where the maximum deflection occurs after the loading point. The relationship between the TSD deflection lag and phase angle of the asphalt concrete (AC) layer was also investigated, and the possibility of estimating pavement conditions from TSD deflection lag was evaluated.

Key Findings

Based on the field data analysis and simulation results, the key findings from this research project were summarized as follows:

- TSD testing is time-efficient, and it is more suitable for network-level pavement evaluation than FWD. The TSD deflection can be used to identify not only weak sections but also weak layers. The deflection indices D0, SCI_12, and D60 correspond to the strength of the entire pavement structure, AC layer, and subgrade, respectively.
- The effects of speed (loading time) and temperature on TSD deflections are equivalent, so the speed effect on pavement responses can be evaluated by the concept of "pseudo temperature." TSD deflection is more sensitive to temperature than speed. At normal TSD driving speeds (20-60 mph), a 10 mph increase in speed is approximately equivalent to a 1°C decrease in temperature.
- The loading frequency of a TSD is lower than that of an FWD, and the AC layer exhibits lower stiffness under a TSD. The TSD deflection basin is steeper than that of the FWD. Based on the simulation results, the TSD-based AASHTO SN is generally smaller than the FWD-based SN (error of 0.74). The TSD-based SN can be calibrated by AC thickness.
- The lag distance increases with increasing fatigue levels until fatigue failure occurs. The lag distance is also related to pavement structures, temperature, and speed. For the same pavement structure, it is possible to identify the fatigued section by comparing the lag distance.
- There is no significant correlation between TSD deflections and pavement performance. Therefore, the value of the TSD lies in its ability to collect pavement structural information, which is not reliably or adequately captured by pavement performance indicators. The combination of using a TSD and pavement performance information allows for more accurate predictions of pavement conditions and more appropriate decisions on maintenance and rehabilitation strategies.

Key Recommendations

Based on the conclusions, the potential recommendations were summarized as follows:

- Due to the limited accuracy of the TSD, it cannot accurately measure deflections when pavement deformation is negligible. Therefore, it is recommended to increase the load magnitude of the TSD or to perform TSD testing during the warm season. In addition, periodic validation of the TSD by other devices such as FWD is recommended for quality control.
- It is recommended that TSD deflections be corrected to the same reference level before performing any analysis. The recommended reference load magnitude, temperature, and speed are 82.2 psi, 20°C, and 40 mph, respectively.
- It is recommended to collect additional and more representative TSD data to calibrate the thresholds of DBPs.

Table of Contents

DISCLAIMER i
Technical Report Documentation Page ii
Acknowledgement iii
Executive Summary iv
Key Findings v
Key Recommendations v
List of Tables viii
List of Figures ix
Glossary of Key Terms and Acronyms x
Chapter 1 Introduction 1
1.1 Problem Statement 1
1.2 Research Objectives 2
1.3 Summary 3
Chapter 2 Literature Review 4
2.1 TSD Measurements 4
2.1.1 TSD deflection 4
2.1.2 Comparisons of TSD and FWD 6
2.1.3 Influencing factor of TSD measurements 6
2.2 Application of TSD Devices 7
2.2.1 Layer modulus 7
2.2.2 Structural capacity 7
2.2.3 Deflection lag 8
Chapter 3 Methodology 10
3.1 TSD Data Collection Guides 10
3.2 FWD Data Collection Guides 11
3.3 3D-Move Simulation 11
3.3.1 Load shape 11
3.3.2 Load magnitude 12
3.3.3 Analysis type 12
3.3.4 Material properties 12
3.4 AASHTO Procedure for Temperature Correction 13
3.4 AASHTO Procedure for SN Calculation 14

3.5 Proposed Speed Correction Method 15
3.6 Deflection Lag Distance Calculation 17
Chapter 4 Results and Discussion 19
4.1 Data Collection and Exploratory Data Analysis 19
4.1.1 TSD 19
4.1.2 FWD 22
4.1.3 Pavement performance 23
4.2 TSD Data Correction Guide 25
4.2.1 Load correction 25
4.2.2 Temperature correction 26
4.2.3 Speed correction 27
4.3 Determining SN with TSD Deflections 31
4.3.1 Simulation results and discussions 31
4.3.2 Sensitivity analysis 32
4.3.3 AASHTO back-calculation analysis 34
4.3.4 TSD-based SN calibration 35
4.4 Correlation Analysis Between Deflection Lag and Fatigue Cracking 37
4.4.1 Phase angle and AC fatigue 37
4.4.2 Influencing factors of lag distance 38
4.4.3 Field lag distance evaluation 40
4.5 Incorporating TSD Data Within PMS 43
4.5.1 Correlation between TSD and pavement performance 43
4.5.2 Structural condition evaluation 45
4.5.3 Incorporating TSD within PMS (PMS & DBPs) 46
Chapter 5 Conclusion 48
References 50
Appendices 53
Appendix A: DOT Survey Summary 53
Appendix B: Additional Figures 58

List of Tables

Table 2-1. Comparison between TSD and FWD testing 6
Table 3-1. Difference in loading mechanism between TSD and FWD 13
Table 4-1. Pavement structure design 25
Table 4-2. Temperature correction for D0 of TSD (AASHTO) 27
Table 4-3. Design factors in the parametric study 31
Table 4-4. The sensitivity of the lag distance to TSD speed 39
Table 4-5. Rank correlation between TSD and pavement performance 45
Table 4-6. Structural strength index threshold values. 45
Table 4-7. Pavement condition assessment benchmark 46
Table 4-8. TSD routes assessment based on PMS 47
Table 4-9. TSD routes assessment based on PMS+DBPs 47

List of Figures

Figure 2-1. TSD truck and doppler lasers 4
Figure 2-2. Schematic diagram of TSD deflection calculation 5
Figure 2-3. Lag: (a) in TSD deflection basin; (b) in dynamic modulus test (phase angle) 9
Figure 2-4. AMPT cyclic fatigue test 9
Figure 3-1. TSD load dimensions 11
Figure 3-2. Adjustment to D0 for AC temperature (AASHTO) 14
Figure 4-1. TSD data collection routes in Tennessee 19
Figure 4-2. D0 comparison for overlapping TSD routes 20
Figure 4-3. TSD deflection map 21
Figure 4-4. TSD deflection comparison in regions 22
Figure 4-5. TSD deflection comparison between different route types 22
Figure 4-6. FWD and TSD deflection comparison 23
Figure 4-7. Pavement performance map 24
Figure 4-8. Pavement performance comparison between regions 25
Figure 4-9. Pavement performance comparison between different route types 25
Figure 4-10. Theoretical TSD deflections at different load magnitudes 26
Figure 4-11. Theoretical TSD deflections at different AC temperatures 27
Figure 4-12. Theoretical TSD deflections at different traffic speeds 28
Figure 4-13. Effective temperature at test speeds 29
Figure 4-14. Speed correction on D0 30
Figure 4-15. Deflection comparison between TSD and FWD: (a) D0; (b) SCI12; (c) SCI_subgrade 32
Figure 4-16. 3D-Move deflections for varying pavement conditions: (a) AC dynamic modulus; (b) base modulus; (c) subgrade modulus; (d) AC thickness; (e) base thickness 33
Figure 4-17. AASHTO SN calculation process: (a) AASHTO subgrade radius; (b) AASHTO subgrade resilient modulus; (c) AASHTO pavement effective modulus 35
Figure 4-18. TSD-based SN: (a) Linear regression; (b) Variable importance of the random forest model; (c) Calibration by AC thickness 37
Figure 4-19. The influence of AC damping ratio on deflection lag 38
Figure 4-20. The influence of pavement structures on lag distances 40
Figure 4-21. Comparison of four interpolation methods 40
Figure 4-22. Relationship between TSD lag distance and fatigue cracking 42
Figure 4-23. Lag distance for cracked pavements 42
Figure 4-24. Lag distance for crack-free pavements 43
Figure 4-25. D0 and pavement performance for all TSD route sections 44
Figure A-1. Temperature comparison for overlapping TSD routes 58
Figure A-2. SCI_12 comparison for overlapping TSD routes 58
Figure A-3. D60 comparison for overlapping TSD routes 59
Figure A-4. Dynamic modulus of the AC layer at 68 °F 59
Figure A-5. The dynamic modulus curves of three plant-produced AC materials at 68 °F 60
Figure A-6. Structural condition assessment in Texas [43] 60

Glossary of Key Terms and Acronyms

TSD: traffic speed deflectometer

FWD: falling weight deflectometer

GPR: ground-penetrating radar

NDT: non-destructive testing

D0: deflection at the loading point, in mils

D*r*: deflection at *r* inches from the loading point, in mils

S*r*: deflection slope at *r* inches from the loading point, in μm/m

SCI_12: structural condition index (D0 – D12), in mils

BCI: base condition index (D12 – D24), in mils

SCI_subgrade: structural condition index of subgrade (D36 – D60), in mils

L.M.: log mile

Chapter 1 Introduction

1.1 Problem Statement

Due to the incompleteness of construction history and the resulting inaccuracy of pavement structure value, it is necessary to adopt innovative technologies to obtain accurate network-level pavement structural data in Tennessee. Recent technological advancements have resulted in the development of continuous deflection-measuring devices including the traffic speed deflectometer (TSD). Since the first prototype device was developed in Denmark in the late 1990s, TSDs have been constantly evolving with new features, but the concept remains the same: a set of Doppler velocity-sensing lasers are mounted on a servo-hydraulic beam close to the rear axle of a semi-truck to measure the deflection velocity of a loaded pavement [2]. Based on the measurements, the deflection velocities are divided by the instantaneous vehicle speed to obtain the deflection slope. The deflection can be obtained by numerical integration of the deflection slope.

Currently, deflection measurements remain the only reliable non-destructive method for determining the structural strength of flexible pavements, and the stationary Falling Weight Deflectometer (FWD) is the most prevailing method used at the project-level to assess pavement structural conditions. Unlike static measurement devices, the TSD is capable of performing deflection surveys at traffic speeds, which provides a safe and efficient tool for collecting network-level pavement structural data [1]. Since the TSD is a relatively new device, it is imperative to compare it with the existing measurement devices to validate its applicability and reliability [1]. In addition, the more widely used one (FWD) usually has sufficiently comprehensive and detailed evaluation systems and methods, but the applicability of the new device (TSD) is yet to verify [2]. Simple replications usually lead to discrepancies. Therefore, a detailed comparison of both the FWD and TSD is required to determine the underlying different mechanisms of them.

TSDs can provide better spatial coverage and efficiency than FWDs. However, some challenges exist as applying TSDs for routine survey works. The accuracy and precision of TSD measurements can be influenced by several internal and external factors, e.g., calibration procedures, wind, TSD speed and temperature during the test, and tire-pavement interaction [4,5]. Therefore, it is necessary to develop a reliable TSD deflection correction procedure, which may include the load or temperature correction for TSD deflections, so that TSD deflections collected at different trips or under different conditions will be comparable. Upon validating the reliability and repeatability of TSD measurements, a framework to incorporate the TSD-measured structural data within pavement management system (PMS) can be presented.

Previous studies are mainly focused on the specific value of deflection, and the potentially useful information from the deflection basin shape is ignored. The viscoelastic nature of asphalt concrete (AC) and the inertial damping of the structure could result in a lag between the time that the TSD tire crosses over the point and the time when the maximum response occurs, which was observed in an FHWA study (FHWA-HRT-15-074) [8]. It can be observed that a lag angle exists between the TSD load and the maximum deflection point in the basin. A similar phenomenon could be found in the dynamic modulus test on asphalt materials, in which the time lag between peaks of the stress and strain could be used to obtain the phase angle of pavement materials.

The value of the modulus decreases rapidly, while the phase angle reaches its maximum value, then followed by a rapid drop [9]. This changing pattern shows that the phase angle has the potential to indicate fatigue failure of the asphalt material. Similar to the phase angle obtained from the laboratory test, the lag angle obtained from a TSD deflection basin may have a close relationship with the phase angle, and serve as an index to indicate pavement conditions in terms of the initiation and growth of cracks [10]. The research team believes that using the lag angle will help to predict pavement conditions and select pavement maintenance and rehabilitation treatments more accurately. However, the lag angle can be affected by vehicle speed, temperature, and pavement structure, and more importantly, a complete deflection basin may not be obtained from the TSD if the Doppler lasers only measure half of the deflection basin before the load. These challenges will be investigated in this study. In summary, information from the deflection basin and the lag angle will be considered in the proposed study to develop the structural condition index that can be incorporated into the TDOT PMS system.

1.2 Research Objectives

The objectives of the research work included:

- Develop TSD data collection and analysis guideline(s) for pavement structural evaluation in Tennessee.
- Obtain network-level pavement structural data in Tennessee using the TSD method.
- Develop a methodology for incorporating TSD structural data into TDOT PMS.

To achieve the above objectives, the UT research team firstly identified TSD routes in Tennessee with the help of TDOT engineers and developed practical field data collection procedures and schedules. Then, the UT research team worked with the Australian Road Research Board (ARRB) to execute the field TSD data survey according to the schedule. Once the TSD field data collection was finished, the research team checked the TSD data and determined test sections for FWD testing. With the help of TDOT Materials and Tests Division engineers, the FWD test was performed to check the deflection for the selected section. Field cores were extracted on the FWD test track and later shipped to the UT-Knoxville Infrastructure Materials Laboratory for laboratory performance testing.

Based on the data collected in Tennessee, the research team analyzed the TSD deflection data. The TSD measurements and the FWD measurements were compared. This evaluation was to assess whether the measurements from the two devices followed similar trends or whether the ranking of pavement sections (from weakest to strongest) based on TSD measurements was compatible with ranking based on FWD measurements.

The effect of load magnitude, test temperature, and test speed on TSD deflections was investigated through numerical simulations. A step-by-step guideline on TSD data correction was developed and TSD deflections should be corrected to the same reference level before any analysis is performed.

The research team also developed a new approach to determine the effective structure number (SN) with TSD measurements by modifying the AASHTO method so that the improved TSD-based SN can be comparable to the existing FWD-based SN records. Mechanistic simulation models were developed based on the 3D-Move program to simulate the loading mechanisms associated

with the TSD and FWD and to obtain a deflection database of a wide range of pavement structures.

In addition, the relationship between the TSD deflection lag and phase angle was investigated through 3D-Move simulations, and the possibility of estimating pavement conditions from TSD deflection lag was evaluated based on field TSD data.

Furthermore, TSD measurements and pavement performance data were compared. The purpose of these comparisons was to incorporate TSD structural data into the PMS to predict pavement conditions and select pavement maintenance and rehabilitation treatments more accurately.

1.3 Summary

This report presents the findings, conclusions, and recommendations from the above stated goals and objectives and is organized as follows:

Chapter 1. Introduction: Presents the study objectives, goals, and report organization.

Chapter 2. Literature Review: Summarizes the literature review and most recent findings.

Chapter 3. Methodology: Details the field trials and analysis methodologies. Details the simulation parameters in the 3D-Move program.

Chapter 4. Results and Discussion: Summarizes the analysis results based on field TSD data and simulation results. Discusses the use of TSD data in the pavement structural evaluation.

Chapter 5. Conclusion: Presents the major findings and conclusions that resulted from the project. Presents recommendations for TSD equipment, data collection, data analysis for network-level PMS applications, and future TSD research.

Chapter 2 Literature Review

2.1 TSD Measurements

In the late 1990s, Greenwood Engineering developed a traffic speed deflectometer (TSD), a continuous deflection measurement device that uses Doppler lasers to measure the vertical pavement deflection velocity at regular traffic speeds [3]. As shown in **Figure 2-1**, the TSD uses a set of Doppler lasers mounted on a servo-hydraulic beam near the rear axle (at the midline of dual tires) to measure the vertical deflection velocity of a loaded pavement [4]. The lasers are mounted at a small angle to measure the horizontal vehicle speed, vertical and horizontal vehicle suspension velocity, and vertical pavement deflection velocity. The last sensor is positioned at about 3.6m in front of the rear axle. This sensor is located outside the deflection bowl and is primarily used as a reference laser, so its response can be used to eliminate unwanted measurements [1].

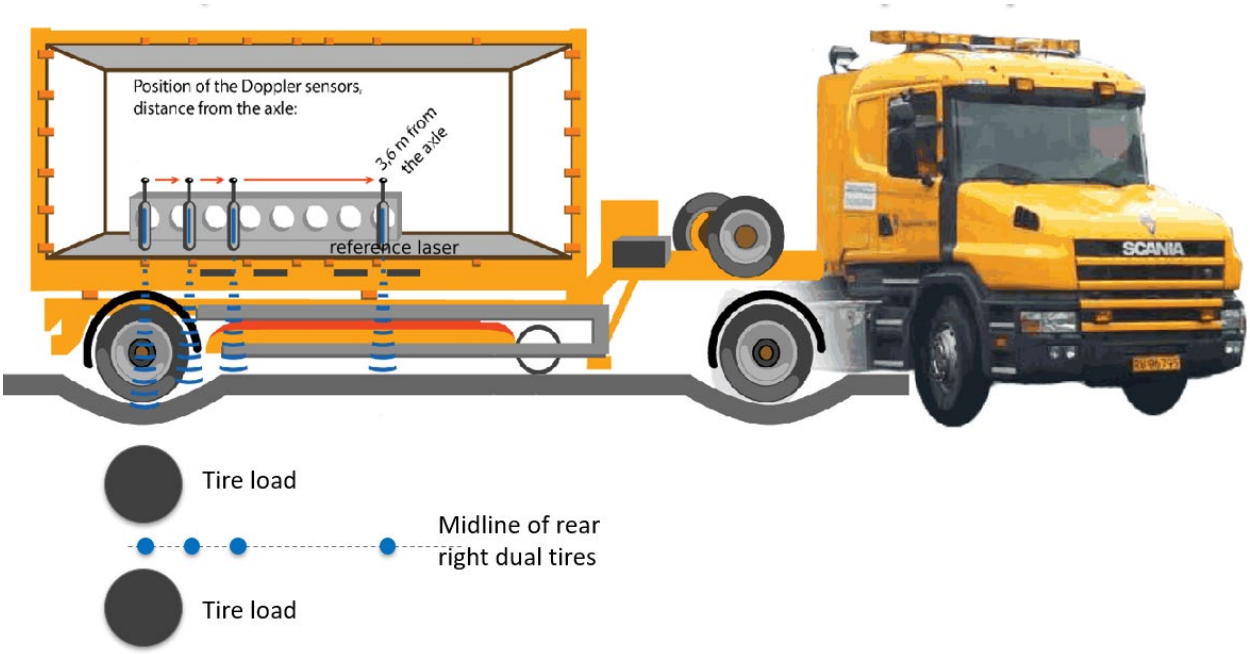

Figure 2-1. **TSD truck and doppler lasers**

2.1.1 TSD deflection

Vertical surface deflection and deflection indices are common parameters used by pavement engineers to represent vertical surface deflection basins. However, the TSD does not directly measure the vertical deflection itself but instead uses discrete Doppler lasers to measure the pavement surface deflection velocity (horizontal and vertical) at traffic speeds. The horizontal proportion of the deflection velocity is related to the moving speed of the TSD. To eliminate the traffic speed dependence of the TSD, the deflection velocity is divided by the instantaneous driving speed to obtain a measurement of the deflection slope. The deflection velocity is measured in μm/s, while the traffic speed is measured in m/s. Therefore, deflection slope measurement is output in μm/m. The deflection slope is then converted to actual pavement

deflection by curve-fitting and numerical integration. The deflection slope is the first derivative of deflections, so the pavement's vertical surface deflection at any given location is the area under the slope curve from the tail to that particular location, as shown in **Figure 2-2**.

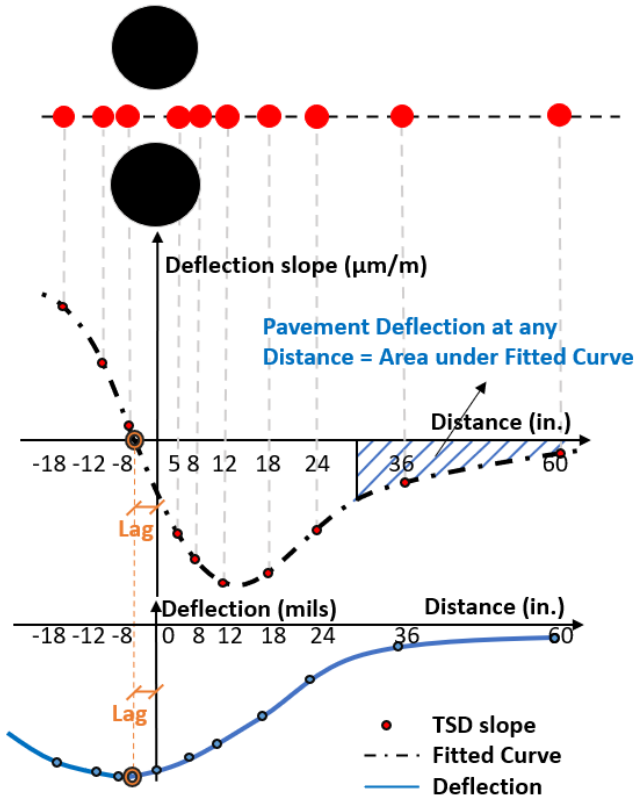

Figure 2-2. **Schematic diagram of TSD deflection calculation**

The deflection algorithm is the method for fitting a continuous curve to measured slope points and calculating the surface deflection, the accuracy of which depends on the suitability of the functional form of the slope curve. Greenwood's TSD deflection algorithm simulates the deflection slope as the sum of Gaussian (symmetric) and stable distribution (asymmetric) functions. Muller and Robert [5] proposed a Piecewise Cubic Hermite Interpolating Polynomial (PCHIP) method. At each interval between two successive measurement locations, different cubic polynomial functions are applied using known function values and derivatives of each location. Since the PCHIP method forces the curve to pass through all data points, it does not exclude or filter out abnormal slope measurements, in which case the PCHIP method can cause serious errors. Zofka et al. [6] presented an approach to calculate surface deflection by integrating the Weibull function fitted by deflection slopes.

In addition, as with most field measurements, TSD data sometimes show anomalous slope measurements related to calibration or measurement problems caused by dynamic loading [7]. It is recommended to use filtering methods to exclude or correct abnormal slopes before applying deflection algorithms. Wix et al. [8] proposed a method to eliminate flat or convex curves by limiting the deflection slope at 900 mm to less than two-thirds of that at the 600 mm.

2.1.2 Comparisons of TSD and FWD

The falling-weight deflectometer (FWD) is a device used to collect pavement vertical deflections in response to an impact load. The FWD drops a heavy weight onto a circular plate placed on the pavement surface to simulate the load of a rolling vehicle wheel. The applied load and vertical pavement deflection at various radial distances from the loading center are measured and recorded [1].

Since the FWD equipment should remain stationary at each test point, lane closures and interruptions to traffic are required. It also limits the productivity of the FWD and the number of test points where measurements can be obtained. A production rate of approximately 2.5 lane-miles per day is typical, assuming testing at a 75-ft interval, which is appropriate for project-level testing [9]. However, issues such as time, expenses, and traffic control hinder FWD testing at the network-level, and the TSD addresses these problems well. The TSD is a continuous deflectometer that operates at normal traffic speed, which can be used to characterize the pavement structural strength efficiently and cost-effectively. The findings of a Federal Highway Administration (FHWA) research project confirmed that TSD measurements meet the accuracy requirements, and the TSD is ready for pavement structure assessment at the network-level [10]. In summary, the use of TSD is both beneficial and economical, especially for network-level PMS applications.

Table 2-1 illustrates the comparison between TSD and FWD testing. The deflection measuring techniques for the FWD and TSD are quite different, and the measured deflection is conceptually different even if the load magnitude is the same. Since most of the current deflection tests are performed using an FWD, it is used as a reference device to evaluate the accuracy of the TSD. However, given the difference between the pavement surface response under the moving TSD and the response generated by an FWD, the FWD may not be a true reference. But although the deflection values are different, it is clear from the visual inspection that both measurements follow the same trend and have the same peak points [1].

Table 2-1. Comparison between TSD and FWD testing

	TSD	*FWD*
Load	moving load	impact load
Measurement	deflection velocity	deflection
Social benefit	• non-destructive • save time • little or no traffic control	• non-destructive • time-consuming • traffic closure
Test scope	network-level	project-level

2.1.3 Influencing factor of TSD measurements

The dynamic load of the vehicle axle includes static load and disturbing load caused by pavement roughness. The ratio of the standard deviation of the dynamic load with respect to the static load varies from 0.05 to 0.3, depending on the vehicle suspension, speed, and pavement roughness. Therefore, the actual dynamic loads applied to the pavement induce surface deflection that may be very different from the static loads. A study reported that there was a significant difference in the coefficient of variation (COV) of TSD measurements for pavements with good ride quality

(reported IRI of 95 in./mi. or less) and pavements with acceptable ride quality (IRI of 170 in./mi. or less) [11], which proved that the pavement roughness significantly affects the deflection of TSD field measurements.

Elseifi et al. [11] conducted TSD tests at 30 mph and 45 mph along a low volume road (LVR) and at 45 mph and 60 mph on the mainline to study the effect of TSD speeds on TSD measurements. Testing at 30 mph along the LVR resulted in a COV of the deflection slope that was approximately 24% lower than those measured at 45 mph. The COVs at 60 mph were approximately 38% higher than that at 45 mph on the mainline. The results suggested that the deflection was sensitive to the moving speed.

2.2 Application of TSD Devices

2.2.1 Layer modulus

The online DOT survey reported that around 71.4% of states typically calculate the pavement layer modulus based on deflection measurements as a key engineering parameter. Available back-calculation tools commonly use linear elastic analysis (LEA) for the pavement layers and only adopt FWD loading characteristics to calculate pavement responses. Due to differences in loading configurations and mechanisms, the applicability of these tools in conjunction with TSD data is still questionable. Some studies show that using FWD-based programs with TSD deflections would result in back-calculated AC and subgrade modulus that are larger than their actual values [12].

Two methods have been used in the literature to perform back-calculation using TSD data. The first method relies on mechanistic pavement response models under moving loads. A recent study used WESLEA and 3D-MOVE programs to back-calculate the elastic layer modulus from the measured deflection slopes from TSD data [3]. The main advantage of this method is the use of TSD deflection slopes. Since TSD deflection slopes are measured directly by TSD testing, this method does not require the use of any algorithm to calculate the surface deflections and is independent of the calculation-related error [3]. However, it is a computationally intensive method that changes the inputs by trial and error to match the 3D-Move output to the TSD measured data, which may be impractical for network-level applications. Wu et al. [13] developed a semi-analytical back-calculation method based on the 2.5D finite element method combined with the Constrained Extended Kalman Filter method. This algorithm is based on the forward analysis of the pavement response affected by moving loads using 2.5D finite elements, which has not been used for pavement analysis before.

Another method is based on the conversion between the FWD deflections and TSD deflections in order to use existing back-calculation tools developed for FWD [11]. Machine learning models were used to convert the TSD deflections to the corresponding FWD deflections. This method showed promising results; however, a large amount of deflection data is needed to develop machine learning models. The accuracy is affected by both the conversion model of TSD/FWD deflections and the back-calculation method for FWD data [11].

2.2.2 Structural capacity

The pavement structural number (SN) is a frequently used index of pavement structural strength due to its applicability and adaptability to various material types and environmental conditions

[14]. Traditionally, the SN of existing pavement structures is estimated from its layer thickness and laboratory-determined material properties, which is destructive, expensive, and not always suitable for large-scale applications [15]. The 1993 AASHTO design guide introduced an approach to determine the effective SN through non-destructive testing (NDT) [16], Falling Weight Deflectometer (FWD) testing, which has been a prevailing method used at the project-level to assess pavement structural conditions [17]. Many highway agencies have adopted FWD and ground-penetrating radar (GPR) to evaluate the structural performance of existing pavements because these two testing techniques can provide FWD deflections that represent the overall structural capability, as well as the layer thickness measured by GPR [18].

One of the primary applications of TSD testing is to evaluate the pavement's effective SN and identify structurally weak spots. The loading characteristics of TSD and FWD devices are different, where the FWD uses a single circular impact load, and the TSD applies a moving load on the pavement through the vehicle's dual tires. Therefore, the pavement response under FWD and TSD testing is different [1], and the SN calculated from FWD and TSD deflections are also different. However, there is currently no satisfactory method to use TSD measurements to determine the pavement SN, and engineers still need to convert the TSD measurements to equivalent FWD values [19] or directly use the FWD-based AASHTO method [18]. Zihan et al. [20] proposed a regression model to estimate SN based on TSD deflections collected in Louisiana and Idaho, but a regression model developed through a small number of measurements hindered its application in a wider range of practices. Nasimifar et al. [21] calibrated Rohde's empirical equation [15] to calculate SN from TSD deflections, but it proved to be significantly affected by the accuracy of GPR thickness. In addition, some states indicated that they currently use FWD deflections combined with the AASHTO SN calculation procedure in their PMS [22], so the SN calculated from TSD measurements may not be comparable to the existing FWD-based SN records in the PMS. Therefore, it is necessary to calibrate the FWD-based AASHTO method to make it more applicable for TSD deflections so that the results can match the existing PMS records.

2.2.3 Deflection lag

Current studies of TSDs have focused on specific deflection values, neglecting potentially useful information about the shape of the deflection basin. The viscoelasticity of the asphalt layer and the inertial damping of the structure may lead to a lag between the time when the TSD tire crosses the point and the time when the maximum response occurs, as observed in an FHWA study [23]. Therefore, there is a lag between the loading point and the point of maximum deflection in the basin, where the maximum deflection occurs to fall after the loading point. **Figure 2-3** shows that the TSD deflection basin is asymmetric, with steeper leading edges and shallower trailing edges.

The lag between load and response was also observed in dynamic modulus tests of viscoelastic materials, in which the time lag between peaks of the stress and strain can be used to obtain the phase angle of the material (**Figure 2-3**(b)). According to the AC cyclic fatigue test, as specified in AASHTO TP 133-19, the curve of the modulus and phase angle versus the loading cycles shows four distinct regions: internal heating, micro-crack formation, crack formation, and sample breakdown. **Figure 2-4** shows that the phase angle increases gradually with the loading cycles as the AC is repeatedly loaded. When the sample starts to break down, the phase angle reaches its

maximum value and then begins to drop rapidly. Such a pattern shows that the phase angle is a good indicator of fatigue failure of the AC material. The failure cycle (N_f) is defined as the cycle in which the phase angle drops sharply after a stable increase during cyclic loading. The lag angle obtained from a TSD deflection basin was found to be closely related to the phase angle of viscoelastic materials; thus, it can serve as an index to indicate pavement conditions in terms of the initiation and growth of cracks. In addition, the lag angle was affected by vehicle speed and pavement structures [24].

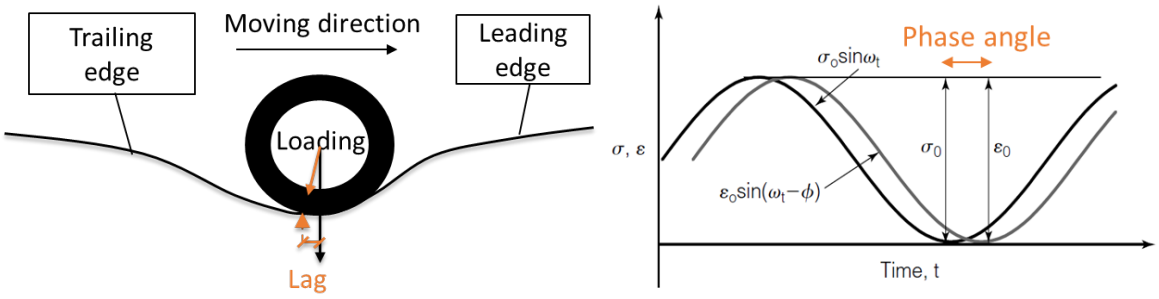

Figure 2-3. **Lag: (a) in TSD deflection basin; (b) in dynamic modulus test (phase angle)**

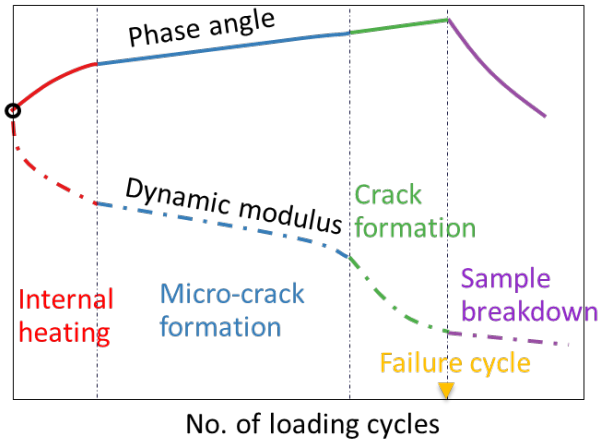

Figure 2-4. **AMPT cyclic fatigue test**

Chapter 3 Methodology

3.1 TSD Data Collection Guides

The device used to measure TSD deflection is the intelligent Pavement Assessment Vehicle (iPAVe) from the Australian Road Research Board (ARRB), a world-renowned road research and technology organization established in 1960. The iPAVe is a fully integrated survey vehicle that collects structural and functional pavement condition data at highway speeds. It collects information including pavement deflection, cracks, longitudinal and transverse road profile, pavement macrotexture, road geometry, etc. The key component of the iPAVe is the TSD equipment, which typically measures at speeds up to 50 mph. The axles are loaded with a maximum weight (load) of 10 metric tons (35,000 lb), nominally 5 tons (17,500 lb.) per wheelset. The TSD applies an approximate 50 kN (11,240 lbf) loading to the pavement.

The TSD uses six Doppler sensors to make slope measurements at 4, 8, 12, 24, and 60 inches from the center of the wheel load. A seventh Doppler laser, referred to as the reference laser, is placed at 138 inches from the load. The upgraded TSD system uses ten Doppler sensors located at -18, -12, -8, 5, 8, 12, 18, 24, 36, and 60 inches from the wheel load center (as shown in **Figure 2-2**), and the reference laser is placed at 121 inches from the load. For the upgraded TSD system, three additional sensors are placed behind the loading center, providing the possibility to estimate the deflection lag.

The iPAVe uses the "Area under the Curve Using Piecewise Cubic Hermite Interpolating Polynomial" (AUTC-PCHIP) method to calculate deflections. This interpolation method applies distinct cubic polynomial functions at each interval between two successive slope measurement locations (thus, it forces the curve to pass through all slope measurements) and then integrates over the length of the deflection bowl. To complete the slope curve and compute the area under the curve, the slopes of the loading point and the reference point are assumed to be zero.

Compared to other deflection tests, iPAVe collects a very large amount of raw data and corresponding processed data (the reported data intervals are 0.01 mile), which includes:

- Measurement: continuous data streams of vertical deflection velocity and horizontal deflection velocity from each sensor location.
- Deflection: averaged deflection based on the AUTC-PCHIP method at the following locations from the load axle in the outer wheel path: 0, 8, 12, 18, 24, 36, 60 and 72 inches (or -18, -12, -8, 0, 8, 12, 18, 24, 36, 60 and 72 inches for the upgraded TSD).
- Temperature: the pavement surface temperature and air temperature with an accuracy of +/-1°F.
- Load: applied axle load, left and right in kg or lbs.
- Pavement performance data: including total cracking, fatigue cracking, longitudinal cracking, transverse cracking, roughness (in international roughness index, IRI), rutting, etc.

3.2 FWD Data Collection Guides

Four drops were made at each test point at a nominal weight of 9,000 lbs. during the FWD data collection. At each drop, the pavement deflection was measured by seven deflection sensors spaced at 0, 8, 12, 18, 24, 36, and 60 inches from the load. The FWD deflection at the test point was the average of the four drops of deflection, excluding the highest and lowest values.

3.3 3D-Move Simulation

To understand the impact of TSD testing characteristics on pavement responses and to find out the underlying differing mechanism between the TSD and FWD, mechanistic simulation models were developed based on the 3D-Move program. Loading mechanisms related to the TSD and FWD were simulated using 3D-Move to obtain corresponding pavement responses.

The 3D-Move program was developed by the University of Nevada, which can be used to simulate pavement responses under moving loads. The program uses the finite layer method and Fourier transform technology to estimate the pavement response [19]. The finite layer method takes advantage of the layered characteristics of the pavement structure, so it becomes an ideal method for studying the pavement response.

Traditional multi-layer elastic programs, such as BISAR3.0, are easy to use, but they cannot accurately simulate pavement responses related to moving loads. Most of them are limited to the static uniform circular loads, while TSD loads need to be defined as moving dual tire loads. Therefore, the 3D-Move model can be more effective and more practical to consider the interaction between the load and the pavement [25]. In addition, 3D-Move allows the incorporation of viscoelastic materials; thus, the AC layer can be simulated as either linear elastic material or viscoelastic material [3]. To characterize the viscoelastic behavior of the AC layer, the dynamic modulus needs to be defined in the 3D-Move program.

TSDs and FWDs differ considerably in multiple facets, not only in the load magnitude and load shape but also in their technologies. Even if the same load is applied to the same pavement structure, the deflection measured by the TSD and FWD are conceptually different. Therefore, a comprehensive comparison is required to ensure that the 3D-Move simulation is realistic and can well reflect the difference between TSDs and FWDs. The notable differences are discussed below and summarized in **Table 3-1**.

3.3.1 Load shape

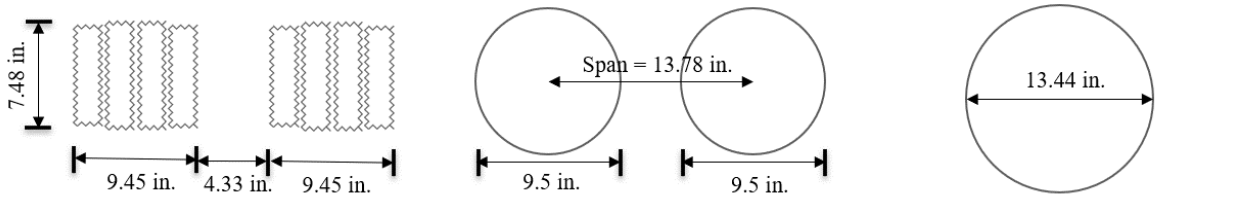

Figure 3-1. **TSD load dimensions**

The contact area of the load applied by an FWD was defined as a circle with a radius of 5.904 inches. For a TSD, the articulated Doppler lasers above the right wheel of the rear axle measure

the deflection velocity along the mid-line between dual tires. The measured values of the tire size are shown in **Figure 3-1**(a) [19], and the equivalent dual and single circular loads are shown in **Figure 3-1**(b) and (c).

3.3.2 Load magnitude

The typical FWD load is nominally 9,000 pounds, and the contact pressure is 82.2 psi. For the moving TSD, due to differences in pavement conditions, the dynamic load magnitude will continuously change during the TSD trip. Therefore, the TSD deflection should be normalized to a standard load level. In this study, the same contact pressure as the FWD (82.2 psi) was used in the TSD simulation. Thus, the total load magnitude of the TSD was approximately 11,660 pounds.

3.3.3 Analysis type

The stationary FWD equipment imposes an impulse load on the pavement surface while the TSD travels at a certain speed and applies loads to the pavement through its rear axle. Therefore, for the stationary FWD, the moving speed should be zero, and it can only be considered by the static analysis of 3D-Move. The impact effect of FWD loading would be represented by the loading frequency, which will be discussed below. For the moving TSD, dynamic analysis was more applicable, and the default moving speed was set to 40 mph.

3.3.4 Material properties

The property of pavement materials is a crucial factor in evaluating the pavement response to applied loads. AC is generally believed as a viscoelastic material, which shows both viscous and elastic properties. The base and subgrade layers were assumed to be linear elastic materials with constant Poisson's ratio. In the 3D-Move program, AC can be defined as a linear elastic or viscoelastic materials, and AC viscoelasticity is characterized by the rate-dependent dynamic modulus curve. Since the rate-dependent dynamic modulus is incorporated by Fourier transform techniques and frequency domain solutions, it is only applicable to the dynamic analysis (moving speed greater than zero). Therefore, the viscoelasticity of the AC layer is not applicable to the FWD simulation (moving speed of zero, static analysis) based on the 3D-Move program. Fortunately, it has been proven that the pavement response was basically linear for a wide range of FWD loads and pavement structures [26]. Meanwhile, the deformation caused by the FWD was considered to be recoverable regarding the instantaneous nature of FWD loading. Therefore, the AC layer was assumed to be linear elastic to the applied FWD load for FWD models. However, the influence of the AC linear elasticity assumption on TSD simulations has not been extensively discussed, and the pavement response under moving loads seems to be more affected by the viscoelastic nature of the AC layer [27]. The dynamic modulus ($|E^*|$) was used to characterize the viscoelastic behavior of the AC layer, which depends on load frequency and temperature.

The equivalent elastic AC modulus was defined as the single dynamic modulus specific to the equivalent load frequency. The determination of the equivalent load frequency of TSDs and FWDs has been a controversial topic with several time-frequency conversion methods [28]–[31]. For FWDs, a typical pulse width is about 30 milliseconds. The most common method is to assume that the frequency of the FWD is calculated as the inverse of the loading time [23]. However, studies showed that the 33.3 Hz ($f = 1/t$) represents the FWD loading frequency at the AC surface, which would result in the underestimation of vertical stress [32]. The equivalent load frequency

of an FWD was recommended to be reduced from 33.3 Hz to a more accurately estimated AC modulus at a specific depth [32]. According to Lytton et al. [28], FWD testing corresponding to a dynamic modulus of the AC layer at a frequency is given by,

$$f = \frac{1}{2t} = 16.7\ Hz \tag{3-1}$$

The equivalent load frequency of 16.7 Hz for FWD was also recommended by the developers of the 3D-Move program [33], which has been verified by full-scale field tests (Penn State University test track and Minnesota road tests) [34]. Therefore, the equivalent loading frequency of FWD was assumed as 16.7 Hz in this study.

For the moving TSD, the current MEPDG approach assumes that the frequency is calculated as the inverse of the loading time (*f = 1/t*) [30], and the loading time is determined according to the following equation:

$$t = \frac{L_{eff}}{17.6\ Vs} \tag{3-2}$$

where *t* is loading time (in seconds), L_{eff} is the effective length (in inches), and V_S is the TSD speed (in mph). The pavement structure determines the effective length. However, recent analytical studies have found that the MEPDG method may underestimate the normal strains relative to the viscoelastic dynamic response [35]. Therefore, the time-frequency conversion method of MEPDG was used in this study, but the effective length (loading time) was calculated differently. The TSD is generally equipped with a reference laser positioned 138 inches away from the loading point, where it is presumed to be relatively unaffected by TSD loading. It is reasonable to assume that the effective length of TSD loading is 276 inches in the longitudinal dimension (both front and rear are 138 inches). According to Equation (3-2), the equivalent load frequency of a TSD moving at 40 mph was approximately 2.6 Hz.

Table 3-1. Difference in loading mechanism between TSD and FWD

Characteristics	*FWD*	*TSD*
Load type	Impulse	Moving
Load shape	Single circular	Dual tires
Load radius	5.904 in.	(Equivalent to) 6.72 in.
Load frequency	16.7Hz	2.6Hz (corresponds to a TSD speed of 40 mph)

3.4 AASHTO Procedure for Temperature Correction

The most commonly used deflection temperature correction method is proposed by the AASHTO design guide, which is based on the deflection at the loading point (D0) of the FWD. As shown in **Figure 3-2**, the temperature correction is achieved by an adjustment factor applied to the raw D0, which varies for different asphalt thicknesses. When the AC temperature is higher than the reference temperature (20°C), the stiffness of the AC layer is weaker than assumed, so the pavement deflections are greater than expected, and the adjustment factor is less than 1.0. The opposite is true when the AC temperature is lower than the reference temperature.

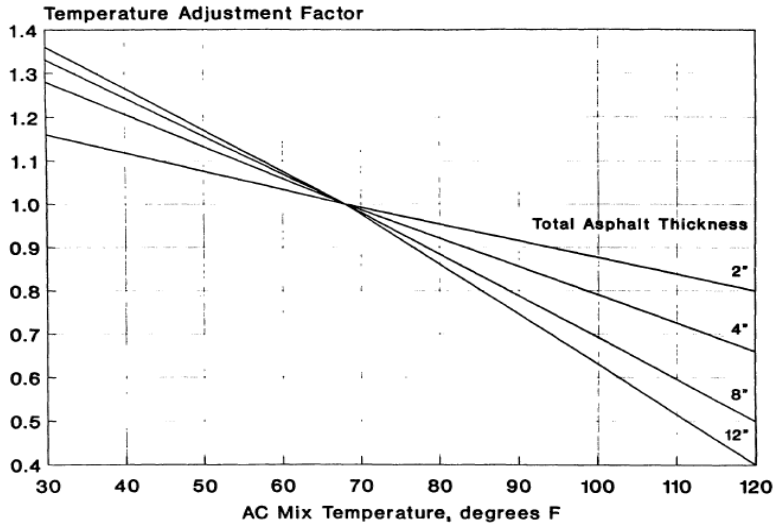

Figure 3-2. **Adjustment to D0 for AC temperature (AASHTO)**

3.4 AASHTO Procedure for SN Calculation

The FWD-based SN calculation procedure proposed in the 1993 AASHTO Pavement Design Guide was widely used in pavement maintenance and rehabilitation to evaluate the structural capacity of existing pavements [16]. With the total thickness of pavement layers and the effective pavement modulus, the effective SN can be obtained with the following equation:

$$SN = 0.0045 * D * \sqrt[3]{E_p} \tag{3-3}$$

where D is the total pavement thickness above the subgrade (inches), E_p is the effective pavement modulus of all layers above the subgrade (psi), and SN is the effective structural number.

The effective pavement modulus represents the overall strength of the pavement layers above the subgrade. The effective pavement modulus can be obtained through the back-calculation analysis of deflections, as well as the subgrade resilient modulus, as shown in Equation (3-4) to (3-6).

$$M_r = \frac{0.24P}{r * d_r} \tag{3-4}$$

Where M_r is the subgrade resilient modulus (psi); P is applied load (lbs); μ is Poisson's ratio; r is subgrade radius, the radial distance at which the deflection is measured (inches); d_r is measured deflection at a radial distance of r (inches).

Given the subgrade resilient modulus and the total thickness of the pavement structure, the effective modulus can be calculated from the deflection measured at the center of the load plate.

$$d_0 = \frac{1.5 * p * a}{M_r}\left[\frac{1}{\sqrt{1+\left(\frac{D}{a}\sqrt[3]{\frac{E_p}{M_r}}\right)^2}} + \frac{\left(1-\frac{1}{\sqrt{1+\left(\frac{D}{a}\right)^2}}\right)}{\frac{E_p}{M_r}}\right] \tag{3-5}$$

where d_0 is the deflection at the center of the load plate (inches), p is the contact pressure (psi), a is the radius of load plate (inches), M_r is the subgrade resilient modulus (psi), D is the total pavement thickness above the subgrade (inches), and E_p is the effective pavement modulus of all layers above the subgrade (psi).

The calculation of the subgrade resilient modulus is based on the fact that, at a point sufficiently far from the loading center, the measured surface deflection is almost entirely due to deformation in the subgrade. In practical applications, the deflection used must be far enough away from the loading center so that the subgrade modulus can be estimated well without being affected by the above pavement layers. It should also be close enough so that the deflection is not too small to be measured accurately.

AASHTO recommends that the selected subgrade radius r in Equation (2) should be greater than seventh-tenths of the effective radius. Additionally, it should also be selected as close as possible to reduce the error caused by the small deviation of the sensor measured value. Therefore, the subgrade radius can be determined from the following relationship:

$$r \geq 0.7\, a_e \tag{3-6}$$

$$a_e = \sqrt{a^2 + \left(D\sqrt[3]{\frac{E_p}{M_r}}\right)^2} \tag{3-7}$$

where a_e is the effective radius, the radius of the stress bulb at the subgrade-pavement interface (inches); a is the circular load radius (inches); D is the total pavement layer thicknesses (inches); E_p is the effective modulus of pavement layer (psi); and M_r is the subgrade resilient modulus (psi).

3.5 Proposed Speed Correction Method

It is well known that the dynamic modulus master curve is developed based on the time-temperature superposition principle and that the effects of loading time (speed) and temperature are equivalent for the AC modulus. Therefore, the time (speed) effect on pavement response can be evaluated by the concept of “pseudo temperature.” Combined with the measured pavement temperature, the time and temperature dependency of AC materials can be integrated into one single factor known as the "effective temperature." In this case, only the effective temperature correction of the TSD deflection is needed to achieve both temperature and speed correction.

According to the MEPDG, the master modulus curve can be mathematically modeled by a sigmoidal function described as:

$$\log|E^*| = \log(Min) + \frac{\log(Max) - \log(Min)}{1 + e^{\beta + \gamma \log w_r}} \tag{3-8}$$

Where $|E^*|$ is the dynamic modulus (ksi); w_r is the reduced frequency (Hz), Max is the limiting maximum modulus (ksi), Min is the limiting minimum modulus (ksi), and β, Y are the fitting parameters.

The reduced frequency is computed using the Arrhenius equation:

$$logw_r = logw + \log\left[a(T)\right] \tag{3-9}$$

$$\log[a(T)] = \frac{\Delta E_a}{19.14714}\left(\frac{1}{T} - \frac{1}{T_r}\right) \quad (3\text{-}10)$$

where *a(T)* is the shift factor at temperature *T*, w_r is the reduced frequency at the reference temperature (Hz), *w* equals loading frequency at the reference temperature (Hz), T_r is the reference temperature (Kelvin), *T* is the test temperature (Kelvin), and ΔE_a is the activation energy, treated as a fitting parameter (J/mol).

The AC modulus at the test speed and test temperature can be equated to the AC modulus at the reference speed and effective temperature. Equation (3-9) can be rewritten as:

$$logw_r = logw_t + \log[a(T_t)] = logw_{ref} + \log\left[a\left(T_{eff}\right)\right] \quad (3\text{-}11)$$

where w_r is the reduced frequency at the reference temperature (Hz), w_t is the loading frequency at the test speed (Hz), w_{ref} is the loading frequency at the reference speed (Hz), T_t is the test temperature at the test speed (Kelvin), and T_{eff} is the effective temperature corresponding to the reference speed (Kelvin).

Substituting equation (3-10) into equation (3-11), the following equation can be obtained, and the effective temperature can be calculated.

$$\frac{1}{T_{eff}} = \frac{1}{T_t} + \left(log\frac{w_t}{w_{ref}}\right) * \frac{19.14714}{\Delta E_a} \quad (3\text{-}12)$$

where w_t is the loading frequency at the test speed (Hz), w_{ref} is the loading frequency at the reference speed (Hz), T_t is the test temperature at the test speed (Kelvin), T_{eff} is the effective temperature corresponding to the reference speed (Kelvin), and ΔE_a is the activation energy (J/mol).

From Equation (3-12), it can be found that the reference temperature is canceled, so the effective temperature is not related to the reference temperature but to the reference speed. Loading frequency is a function of loading speed (time), and its determination has always been a controversial topic. There are several different time-to-frequency conversion methods and choosing an appropriate one can be very difficult. However, the effective temperature is not directly related to the loading frequency but rather to the ratio of w_t to w_{ref}, which can be calculated from the following form:

$$\frac{w_t}{w_{ref}} = \frac{V_t}{V_{ref}} \quad (3\text{-}13)$$

where w_t is the loading frequency at the test speed (Hz), w_{ref} is the loading frequency at the reference speed (Hz), V_t is the test speed (mph) and V_{ref} is the reference speed (mph).

Substituting equation (3-13) into equation (3-12), the effective temperature can be calculated as:

$$\frac{1}{T_{eff}} = \frac{1}{T_t} + \left(log\frac{V_t}{V_{ref}}\right) * \frac{19.14714}{\Delta E_a} \quad (3\text{-}14)$$

where V_t is the test speed (mph), V_{ref} is the reference speed (mph), T_t is the test temperature at the test speed (Kelvin), T_{eff} is the effective temperature corresponding to the reference speed (Kelvin), and ΔE_a is the activation energy, J/mol.

The pseudo temperature (T_s) caused by the difference between the test speed and the reference speed is obtained by

$$T_s = T_{eff} - T_t \tag{3-15}$$

Therefore, the proposed method avoids the common errors caused by time-to-frequency conversion and is, therefore, more concise and trustworthy. The ΔE_a depends on the AC material. Pellinen et al. measured an average activation energy of 205000 J/mol for the unmodified mixture and 202000 J/mol for the modified mixture [36]. Therefore, the default value for ΔE_a was set to the approximate 200000 J/mol.

3.6 Deflection Lag Distance Calculation

The time lag between the peaks of stress and strain was used to obtain the phase angle and dynamic modulus representing the viscoelasticity of the material [20]. The phase angle between the stress and strain is defined as:

$$\varphi = 2\pi \frac{\Delta t}{T} \tag{3-16}$$

where Φ is the phase angle of the material, Δt is the time lag between peaks of the stress and strain within one cycle, and T is the period of the cyclic load. Similarly, the lag angle in TSD deflections can be defined as follows:

$$\varphi' = 2\pi \frac{\Delta l}{L} \tag{3-17}$$

where Φ' is the lag angle in the deflection basin, Δl is the lag distance between the centerline of the TSD load and maximum deflection, and L is the length of the deflection basin. The lag distance in TSD deflections is defined as the distance between the loading point and the maximum deflection point in the basin. Since the deflection slope is the first-order derivative of the deflection, the maximum deflection position is exactly where the TSD slope is zero. Therefore, the lag distance can be calculated by identifying the maximum deflection point or by identifying the zero-slope point.

- Maximum deflection method:
  - Fit the TSD slope curve.
  - Integrate the TSD slope curve to obtain TSD deflection in discrete points.
  - Fit the TSD deflection curve.
  - Determine the maximum deflection point.
- Zero-slope method:
  - Fit the TSD slope curve.
  - Determine the zero-slope point.

As mentioned earlier, the TSD does not directly measure the deflection itself but rather the vertical deflection velocity at traffic speeds. The TSD slope is the raw measurement, while the TSD deflection is calculated by fitting the TSD slope curve and then integrating it. Using the TSD deflection to calculate the lag distance will aggregate the error caused by the curve fitting. In addition, the accuracy of determining the maximum deflection point depends mainly on the fitted deflection curve in the interval near it. However, the TSD deflection curve is not monotonic within this interval, which increases the difficulty of the curve fitting and also limits the choice of fitting methods. In contrast, the fitting of the TSD slope curve is included in the deflection calculation and requires no additional work. The TSD slope curve is monotonic near the zero-

slope point, and its determination is relatively easy. Therefore, the slope method was adopted rather than the deflection method due to its simplicity and accuracy.

The most important step to accurately calculate the lag distance is curve fitting. Typically, curve fitting is the process of constructing a curve or a predefined mathematical function, and the parameters are selected by fitting the function to the TSD slopes. However, the shape of the TSD slope curve is very complex, and it is not symmetric about the loading point due to the presence of deflection lag. It is also not symmetric about the zero-slope point, because the TSD deflection basin itself is asymmetric (with steep leading edges and shallow trailing edges). It is challenging to construct a mathematical function that fits the TSD slope well. Even if successful, this mathematical function must include many unknown parameters. Considering the limited number of TSD Doppler sensors (slope measurements), fitting many unknown parameters is unrealistic. Most TSD slope curve fitting methods either ignore the deflection lag or assume that the TSD slope is symmetric (Zofka et al. [6]). The Greenwood method is the best-known curve fitting method for TSD slopes, which simulates the deflection slope as the summation of symmetric (Gaussian) and asymmetric (stable distribution) functions but remains proprietary to its details.

The interpolation method is commonly used to fit complex curves. Distinct polynomial functions are applied at each interval between two successive measurement locations. Four interpolation methods (polynomial functions) with different levels of complexity are listed below:

- Linear: Linear spline interpolation
- Spline: Cubic spline interpolation
- Pchip: Piecewise Cubic Hermite Interpolation Polynomial
- Makima: Modified Akima piecewise cubic Hermite interpolation

Of these, linear spline interpolation is the simplest, connecting adjacent TSD slope measurements by straight lines. For the TSD sensors configuration shown in **Figure 2-2**, the lag distance (Δl, in inches) can be calculated as:

$$\frac{|5|+\Delta l}{|-8|-\Delta l} = \frac{|S5|}{|S.8|} \tag{3-18}$$

The slope at location *r* is defined as S*r*, so S5 means the deflection slope at 5 inches in front from the TSD load center, and S.8 means the deflection slope at 8 inches behind the load center. The Spline, Pchip, and Makima methods all perform different forms of piecewise cubic interpolation. Each method differs in how it calculates the interpolant's slope, leading to different behaviors when the underlying data has flat areas or undulations [37].

As shown in Equation (3-17), the lag angle of the deflection basin is related not only to the lag distance but also to the length of the deflection basin. However, the latter is very difficult to estimate accurately in practice. The farthest sensor on the TSD is located 60 inches from the loading center, which is far from the end of the deflection basin (normally, it would be 138 inches). Calculating the length of the deflection basin implies the use of the fitted curve that is beyond the range of the observed data, which has a large degree of uncertainty. Therefore, to avoid introducing additional errors in the lag calculation, only the lag distance was considered in the subsequent analysis.

Chapter 4 Results and Discussion

4.1 Data Collection and Exploratory Data Analysis

4.1.1 TSD

4.1.1.1 TSD data collection routes

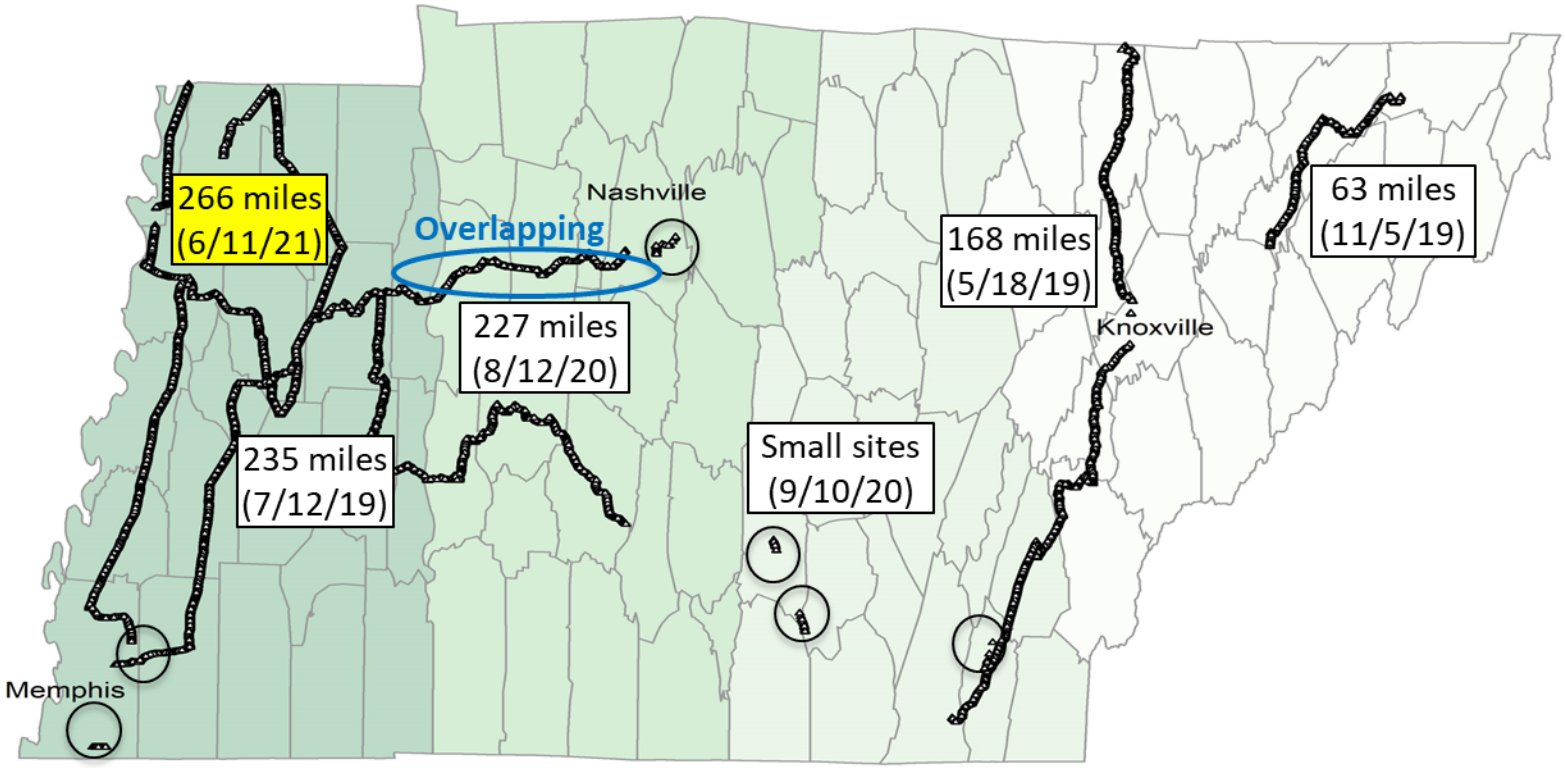

Figure 4-1. **TSD data collection routes in Tennessee**

TSD data were collected multiple times throughout Tennessee from 2019 to 2021, with data collection routes and timing shown in **Figure 4-1**. In 2019, TSD data were collected three times in eastern (63 miles), central (168 miles), and western (235 miles) Tennessee. About 227 miles of TSD data were collected in 2020, with approximately 80 miles of the TSD route overlapping with the 2019 route. Besides, TSD data were also collected in some small sites in 2020. In 2021, ARRB upgraded their TSD devices by installing additional Doppler sensors behind the right rear tire (loading point), providing the possibility to estimate the deflection lag. About 266 miles of TSD data were collected in western Tennessee using the upgraded TSD device in 2021. A total of about 959 miles of TSD data were collected in Tennessee.

4.1.1.2 Overlapping TSD routes

There were approximately 80 miles of 7 route segments of overlapping TSD routes to verify the repeatability of the TSD deflection data. TSD data for the overlapping TSD routes were collected on July 12, 2019, and August 12, 2020, respectively. The air temperature of the two trips were very close to each other, with a difference of less than 10 °F (in Appendices **Figure A-1**). However, the measured deflections of the two TSD trips are significantly different. **Figure 4-2** shows the comparison of D0 for the overlapping TSD routes, and all deflections were corrected to the same load magnitude. Deflection at *r* inches from the loading point is defined as Dr. SCI_12 is defined as the difference between D0 and D12, and BCI is defined as the difference between D12 and D24.

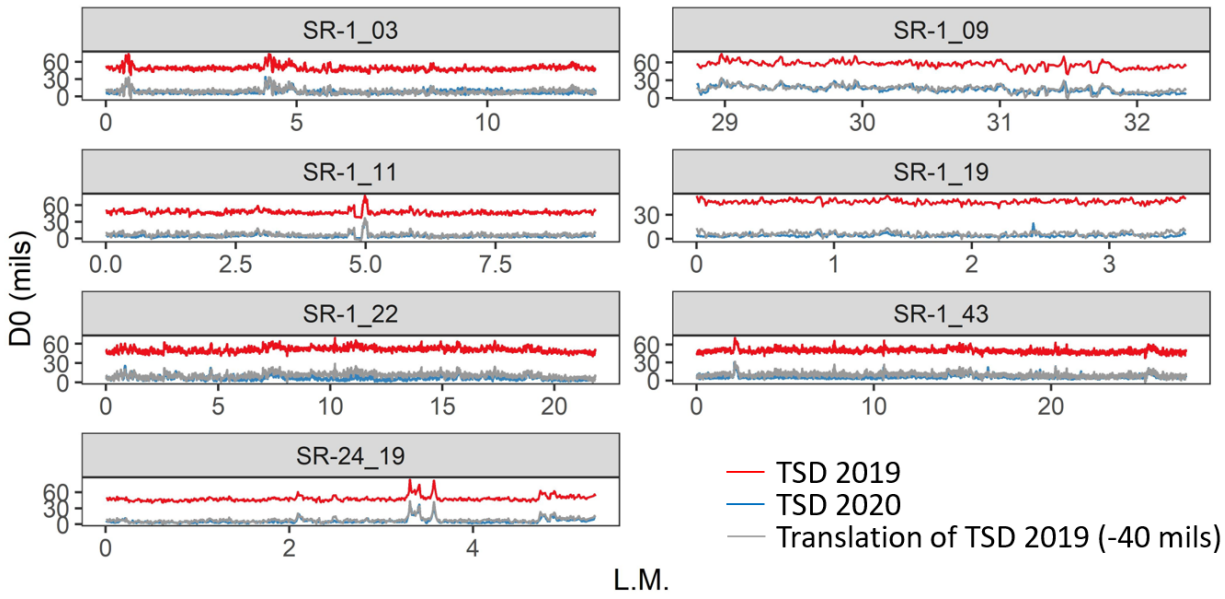

Figure 4-2. **D0 comparison for overlapping TSD routes**

The comparison of SCI_12 (**Figure A-2**) and D60 (**Figure A-3**) is presented in Appendices. The deflections in 2019 are much larger than those in 2020, but they followed the same trend and have the same peak points. If the D0 in 2019 is shifted by 40 mils, it will match the 2020 D0 well. Since deflections in overlapping routes have the same peak points and almost constant deviations, the significant difference is considered to be caused by the TSD device calibration. The ARRB explained that the TSD data collected on July 12, 2019, were affected by the beam

misalignment of the TSD device. Therefore, TSD data collected on July 12, 2019, were excluded from the subsequent analysis by default. Overall, the reliability and repeatability of the raw TSD deflection have yet to be verified, but the TSD deflection of the same trip is meaningful and can be used to identify strong and weak sections.

4.1.1.3 Exploratory TSD data analysis

Figure 4-3 shows the TSD deflection maps for D0, SCI_12, BCI, and D60 in Tennessee, corresponding to the strength of the entire pavement structure, AC layer, base layer, and subgrade respectively. The higher deflection index indicates the weaker structural strength of the pavement layer. The median value of each index for each section is marked with a triangle, and its value is indicated by the size of the triangle. The top 10 sections with the highest deflection index are highlighted in red, indicating the structurally weak sections. Invalid TSD data collected on July 12, 2019 (affected by the beam misalignment) are marked in white and are not included in the ranking. It can be found that the road sections with relatively weak pavement structures are mainly located in West Tennessee, and there are also some road sections with relatively weak pavement structure in East Tennessee. The top 10 highest D60 sections are all located in West Tennessee, indicating a significantly weaker subgrade than the rest of Tennessee.

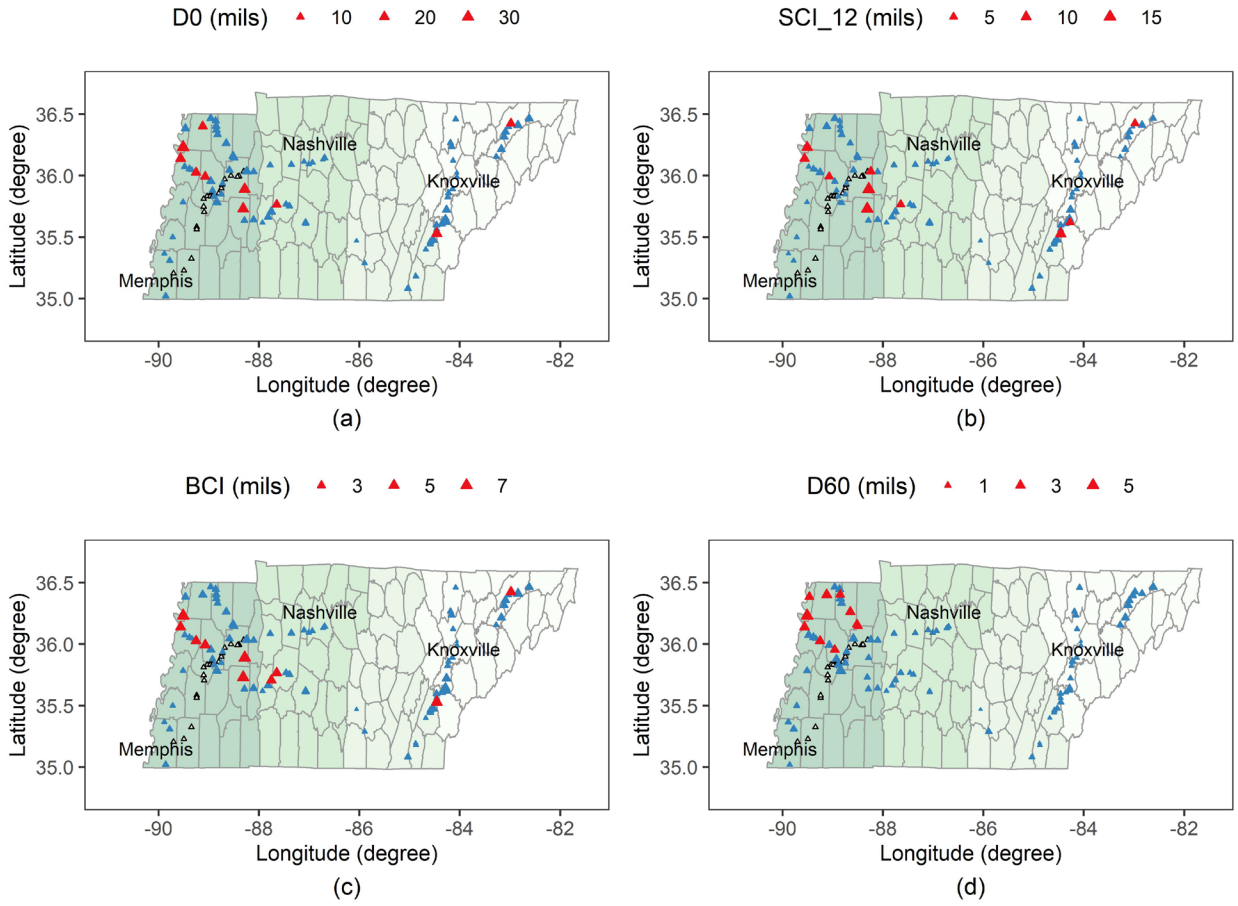

Figure 4-3. **TSD deflection map**

In **Figure 4-3**, the four regions of Tennessee from east to west are shaded in different colors, and a comparison of the TSD deflection indices for the four Regions is shown in **Figure 4-4**. It can be found that the D0 of region 4 is slightly higher than the D0 of Region 1, while the D0's of Regions 2 & 3 are the smallest. However, SCI_12 is almost the same in all regions, indicating that there is no significant difference in the AC layer (thickness and strength) in different regions. Regions 1&4 show greater BCI compared to Regions 2 & 3. In addition, the D60 of Region 4 is significantly greater than other regions. This indicates that the larger deflection in Region 4 is mainly from the larger subgrade deformation (D60) and that the subgrade in Region 4 is softer than other regions.

Figure 4-5 compares the TSD deflection indices for different types of routes in Tennessee using boxplots. The boxplot displays the distribution and skewness of numerical data through the data quartiles, including the minimum, first quartile, median, third quartile, and maximum. It can be found that D0, SCI_12 and BCI are smaller on the interstates compared to the state routes (SR), indicating that the AC layer is stronger on the interstates. This can be explained by the fact that the AC layer of the interstate is always thicker than that of the SR. However, **Figure 4-5**(d) shows that D60 is significantly higher on the interstates than on SR. This should be attributed to the fact that 86% of the interstates on the TSD routes are in region 4, where the subgrade is softer (larger D60). It also indicates that the route types on the TSD routes are unevenly distributed and not well represented.

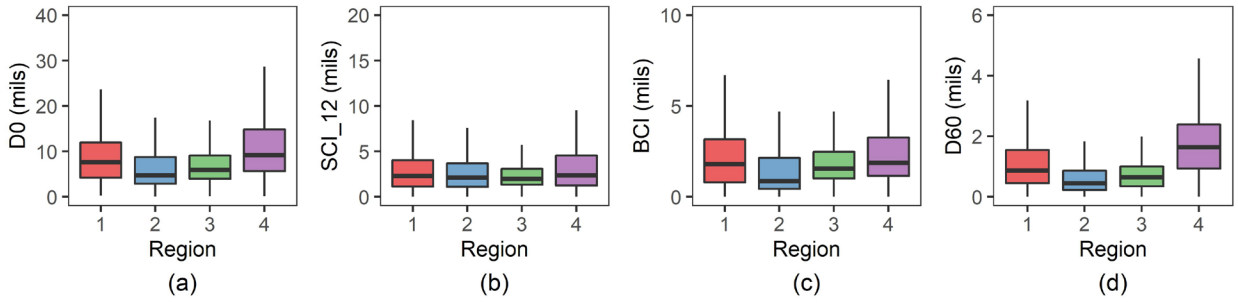

Figure 4-4. **TSD deflection comparison in regions**

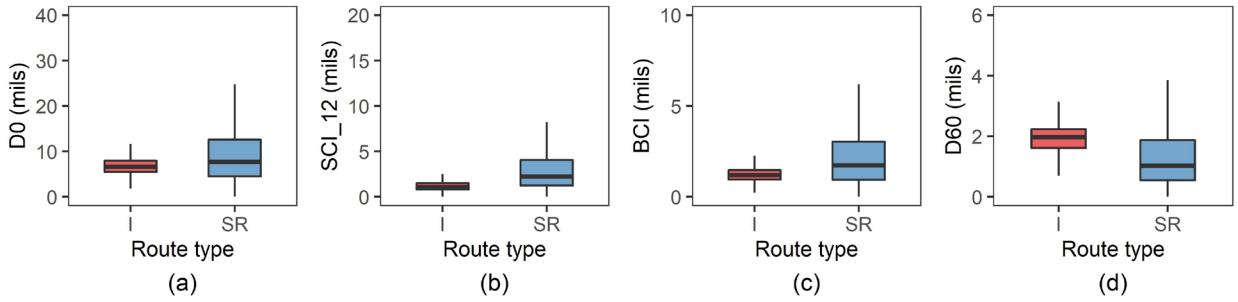

Figure 4-5. **TSD deflection comparison between different route types**

4.1.2 FWD

FWD testing was conducted on seven state routes in Tennessee that overlap with GPR and TSD routes. FWD deflections were collected for 104 test sites, and nine core samples were obtained. In addition, TDOT provided additional FWD deflection information for 86 test points on SR-194_24

in Fayette County. After combining the TSD and GPR data, there were a total of 168 valid FWD and TSD pairs (FWD data collected on SR-187_24 was excluded due to their invalid TSD data).

The deflection comparison between TSD and FWD data is shown in **Figure 4-6**, where FWD deflections are represented by points and TSD deflections are represented by straight lines. The TSD deflection is the average of 0.01-mile intervals, while the FWD deflection is the deflection at certain fixed points. All TSD and FWD deflections were corrected to the same load magnitude (82.2 psi). Combined with the GPR thickness information, both D0 and SCI_12 were corrected to the reference temperature (68 °F). It can be found that the D0 of the FWD and TSD tests are different because of different loading mechanisms. The D0 of the TSD was sometimes larger and sometimes smaller than the D0 of the FWD, but they seem to follow a similar trend. When the deflection was small, the D0 measured by the FWD was always larger than the D0 measured by the TSD. This may be due to the limited accuracy of TSDs, which cannot measure the deflection with sufficient accuracy when the pavement deformation is negligible. Therefore, it is recommended to increase the load magnitude of the TSD or to perform TSD testing in the warm season.

The SCI_12 of the TSD was always greater than SCI_12 of the FWD, except in cases of very small SCI, which may indicate that the viscoelastic AC layer exhibits lower stiffness (lower loading frequency) under TSD than under FWD testing. The opposite is true for D60, which was always smaller for the TSD, indicating that the deflection basin from TSD testing is steeper than that of FWD testing.

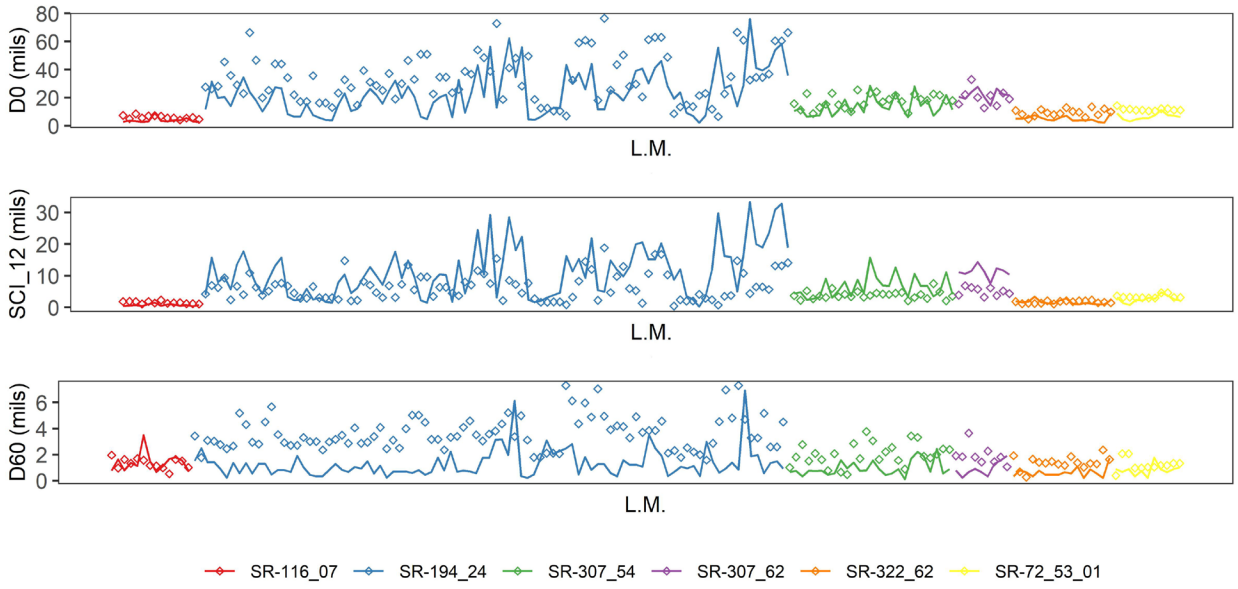

Figure 4-6. **FWD and TSD deflection comparison**

4.1.3 Pavement performance

In addition to deflections, the TSD device also collects pavement performance (functional condition) information simultaneously. **Figure 4-7** shows the pavement performance maps of the TSD routes in terms of IRI, total cracking, fatigue cracking, and rutting. Similar to **Figure 4-3**, the median value of each indicator for each section is marked as the triangle and scaled by its

value. The highlighted (red) top 10 sections have the highest pavement performance indicator, indicating their relatively poorer pavement performance. Invalid TSD routes (affected by the beam misalignment) are marked in white and are not included in the ranking. It can be found that the severely distressed sections are mainly located in West Tennessee, with only a few distressing points in East Tennessee. The top 10 most fatigued sections were all located in West Tennessee, while fatigue cracking was rare in East Tennessee.

A comparison of the pavement performance for the four regions is shown in **Figure 4-8**. For all pavement performance indicators, the median value of the sections in Region 4 is higher than that of the sections in other Regions. In particular, there are more fatigue cracks in Region 4, while there were almost no fatigue cracks in other Regions. Slightly less distress occurred in Region 3 than in Regions 1 & 2.

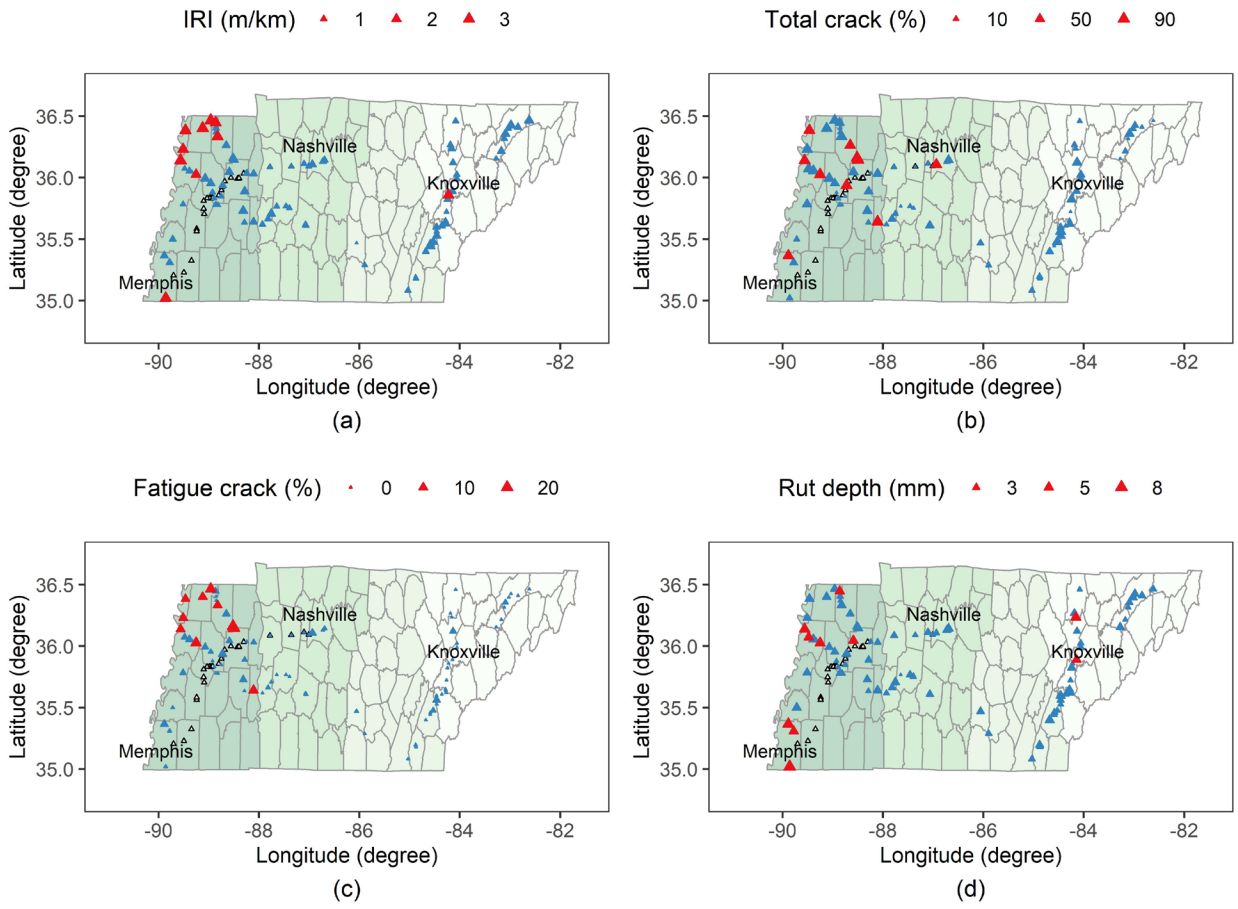

Figure 4-7. **Pavement performance map**

Figure 4-9 shows the comparison of pavement performance for different route types in Tennessee. It can be found that the interstate shows a smaller IRI than SR. However, the total crack, fatigue crack and rutting are greater on interstates than on SR. This may also be due to the uneven distribution of route types on the TSD routes, with most of the interstates being in Region 4.

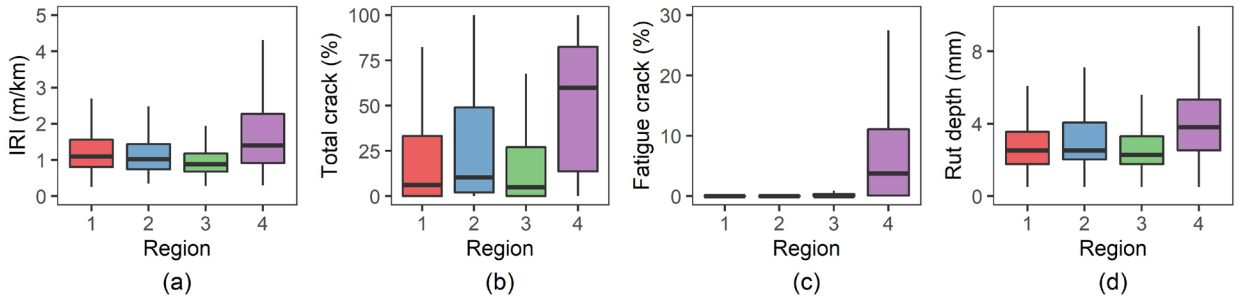

Figure 4-8. **Pavement performance comparison between regions**

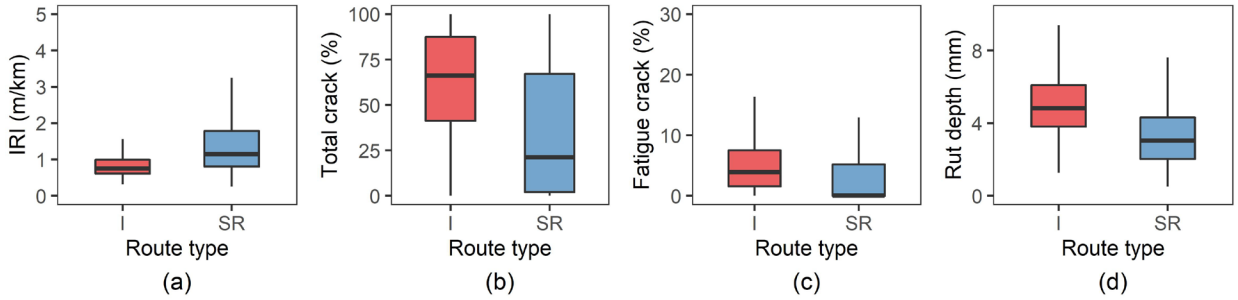

Figure 4-9. **Pavement performance comparison between different route types**

4.2 TSD Data Correction Guide

The load magnitude directly affects pavement deflections. The TSD nominally applies a load of approximately 50 kN (11,240 lbs) on the pavement, while travel and pavement conditions may influence its actual load. In addition, due to the viscoelasticity of the AC layer, the TSD deflection is affected by temperature and the TSD speed. To investigate the sensitivity of TSD deflection to load, temperature, and speed, TSD models of a three-layer pavement structure were developed using the 3D-Move program, as shown in **Table 4-1**. A typical plant-produced AC in Tennessee was used as the AC layer, and the viscoelasticity of AC was incorporated through the dynamic modulus (temperature and frequency-dependent). The dynamic modulus curve for the AC layer is presented in Appendices **Figure A-4**.

Table 4-1. Pavement structure design

Layers	*Thickness (inch)*	*Modulus (ksi)*	*Poisson's ratio*	*Damping ratio*
AC	8	n/a	0.30	25%
Base	9	30	0.35	0
Subgrade	n/a	20	0.40	0

4.2.1 Load correction

A sensitivity analysis was conducted to investigate the effect of the magnitude on TSD deflections, considering three levels of TSD load magnitude of 115psi, 125 psi, and 134 psi. Obviously, the greater the load magnitude, the greater the TSD deflections, as shown in **Figure 4-10**. All TSD deflections are corrected to the same load magnitude of 134 psi through load correction (simply multiplying by its multiplier). It can be found that even under the assumption of moving dual

circular load and viscoelastic AC, the influence of load magnitude can be eliminated by the load correction.

Therefore, TSD deflections should be normalized to the same reference load magnitude (a standard load level) before any analysis is performed. The recommended reference load magnitude is 82.2 psi, which is the nominal contact pressure of an FWD, so that the TSD and FWD deflections can be comparable.

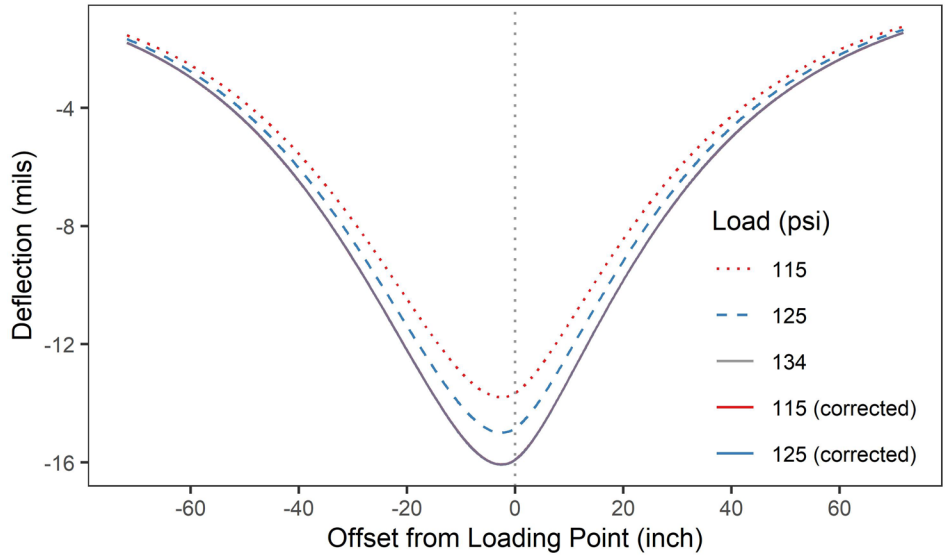

Figure 4-10. **Theoretical TSD deflections at different load magnitudes**

4.2.2 Temperature correction

To study the effect of temperature on TSD deflections, seven AC temperatures were considered: 10, 18, 19, 20, 21, 22, and 30°C. The theoretical TSD deflections at different AC temperatures are shown in **Figure 4-11**. It can be found that the TSD deflection near the loading point increases with the increase of temperature. In addition, deflections near the loading point are more sensitive to temperature than deflections at distant locations. When the temperatures are similar, there is no significant difference in the deflection at the far end. When there is a large temperature change, distant deflections differ significantly.

Therefore, it is necessary to correct TSD deflections to the same reference temperature so that the TSD deflections collected at different temperatures can be comparable. However, there are currently no available methods for temperature correction of TSD deflections. The most commonly used temperature correction method proposed by the AASHTO is based on FWD deflections, and its applicability to the TSD remains to be verified. Besides, the AASHTO method is only for D0.

The following results (**Table 4-2**) are obtained by applying this method to D0 of the TSD and assuming D0 at 20°C as the reference value. It can be found that the difference in D0 is well corrected for both temperatures close to 20°C and temperatures that differ significantly from 20°C. The difference (evaluated with root mean square error (RMSE), as shown in Equation (4-1))

in D0 caused by the AC temperature is reduced from 1.43 mils to 0.10 mils. Therefore, the AASHTO temperature correction method can be used for the D0 of the TSD.

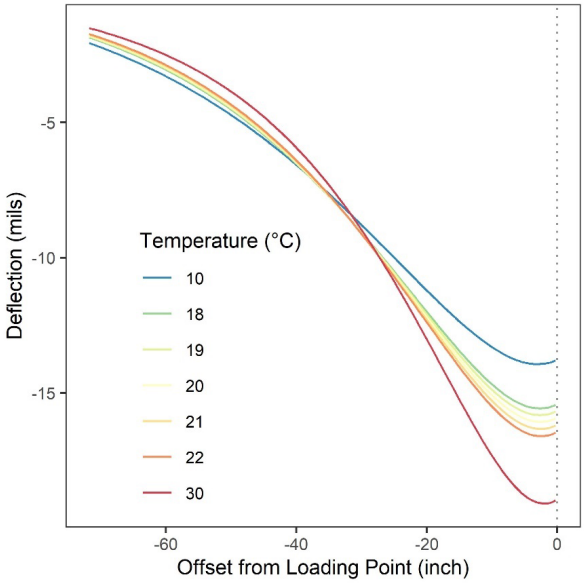

Figure 4-11. **Theoretical TSD deflections at different AC temperatures**

In addition, the AASHTO temperature correction method was also applied to SCI_12 of the TSD, using the same adjustment factor as D0. There is a small improvement in the SCI_12, where the difference in SCI_12 caused by AC temperature is reduced from 0.56 mils to 0.21 mils. It should be noted that the corrected SCI_12 is obtained by applying the same adjustment factor to both D0 and D12. The SCI_12 calculated from the corrected D0 and the raw D12 will result in a large error (RMSE of 0.96 mils).

Table 4-2. Temperature correction for D0 of TSD (AASHTO)

Test Temperature (°C)	*10*	*18*	*19*	*20*	*21*	*22*	*30*	*RMSE (mils)*
Raw D0 (mils)	13.78	15.41	15.66	15.91	16.17	16.44	18.94	1.43
Corrected D0 (mils)	15.73	15.89	15.90	15.91	15.89	15.87	15.66	0.10
Raw SCI_12 (mils)	2.70	3.23	3.32	3.41	3.50	3.61	4.67	0.56
Corrected SCI_12 (mils)	3.12	3.33	3.37	3.41	3.44	3.48	3.86	0.21

$$RMSE = \sqrt{\frac{1}{n}\sum_{k=1}^{n}(y_k - \hat{y}_k)^2} \quad (4\text{-}1)$$

Where y_k is the reference value; $\hat{y}_k$ is the predictions.

4.2.3 Speed correction

4.2.3.1 Sensitivity analysis of TSD speeds

Since the dynamic modulus of the AC layer depends not only on the temperature but also on the loading frequency, the TSD speed may also affect the TSD deflection. Based on the same pavement structures listed in **Table 4-1**, TSD models with different speeds were developed using

the 3D-Move program. The theoretical TSD deflections at different speeds are shown in **Figure 4-12**. It can be found that D0 increases as the TSD speed decreases, while the opposite is true for the distant deflection. This can be explained by the fact that the loading frequency increases with the increasing TSD speed, and the AC layer exhibits higher stiffness, so the D0 decreases. In addition, TSD deflections are more sensitive to lower traffic speeds, while the difference between higher speeds is relatively insignificant. It may arise from the nonlinear relationship between the dynamic modulus and the loading frequency. Overall, the sensitivity of TSD deflections to TSD speed is lower than that of AC temperatures.

The TSD travels at traffic speed, which varies according to different pavement grades and traffic conditions. In addition, the TSD may move slowly due to traffic jams or even stop due to traffic signals. Therefore, it is necessary to set a reference speed and develop a speed correction method for TSD deflections. The TSD deflection should be corrected to the same reference speed so that all TSD deflections measured at different speeds can be compared. However, due to the fixed loading time of the stationary deflectometer, the speed correction of deflections, unlike the temperature correction, has rarely been studied.

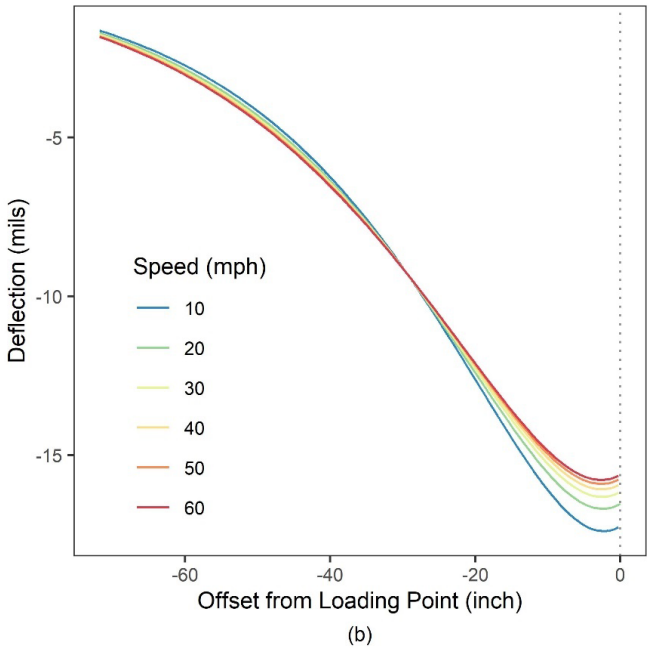

Figure 4-12. **Theoretical TSD deflections at different traffic speeds**

4.2.3.2 Speed correction method

As mentioned in previous chapters, according to the time-temperature superposition principle, the time (speed) effect on pavement response can be evaluated by “pseudo temperature.” Therefore, the combined effects of speed and test temperature can be integrated into one factor known as the "effective temperature." According to Equation (3-14), the effective temperature for different TSD speeds at any test temperature can be calculated.

Assuming a test temperature of 20 °C and the reference speed of 40 mph, the effective temperature for different TSD testing speeds is shown in **Figure 4-13**. The effect of the choice of the reference speed on the effective temperature is also explored. It can be found that when the

test speed is exactly equal to the reference speed, the effective temperature is the test temperature. When the test speed is lower than the reference speed, the pseudo temperature caused by the test speed is positive, so the effective temperature is greater than the test temperature. Conversely, when the test speed is greater than the reference speed, a negative pseudo temperature occurs, and the effective temperature is smaller than the test temperature. In general, as the test speed increases, the pseudo temperature decreases, and so does the effective temperature. In addition, for the same test speed, the lower the reference speed, the lower the pseudo temperature, and the lower the effective temperature. Since the effective temperature is independent of the reference temperature, the results are the same regardless of the choice of reference temperature. In addition, at normal TSD driving speeds (30-60 mph), the effect of a 10-mph speed change is approximately equivalent to the effect of a 1°C temperature change.

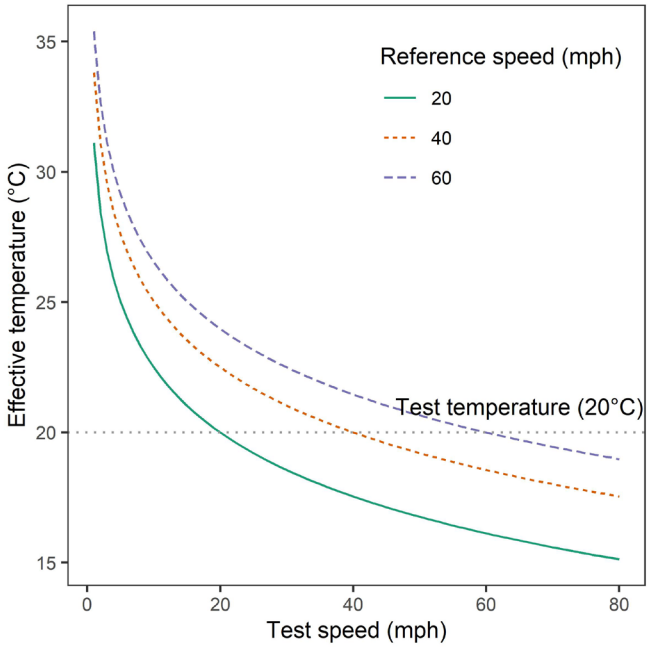

Figure 4-13. **Effective temperature at test speeds**

4.2.3.3 Application of the proposed method

Due to the equivalence of the AC modulus, the TSD deflections at the test speed and test temperature are equal to the TSD deflections at the reference speed and effective temperature. Afterward, the latter can be corrected to the reference temperature (and, of course, to the reference speed) according to the AASHTO temperature correction method, whose applicability has been verified in the previous section. In this way, the TSD deflections at different speeds and different temperatures can be comparable. It should be noted that the effective temperature combines the effects of test speed and test temperature. Speed correction and temperature correction are achieved simultaneously rather than sequentially. The detailed procedure for TSD deflection correction is:

Step 1: Determine the reference load magnitude, reference speed, and reference temperature.

Step 2: Input the TSD deflections, load magnitude, test speed, and test temperature.

Step 3: Input the thickness of the AC layer. (Optional: Input the AC dynamic modulus master curve function or ΔE_a).

Step 4: Correct TSD deflections to the reference load magnitude.

Step 5: Calculate the effective temperature based on test speed and test temperature using Equation (3-14).

Step 6: Obtain the adjustment factor for the effective temperature based on AC thickness according to the AASHTO temperature correction method.

Step 7: Apply the adjustment factor to the load-corrected D0 of the TSD to obtain the speed-and temperature-corrected D0.

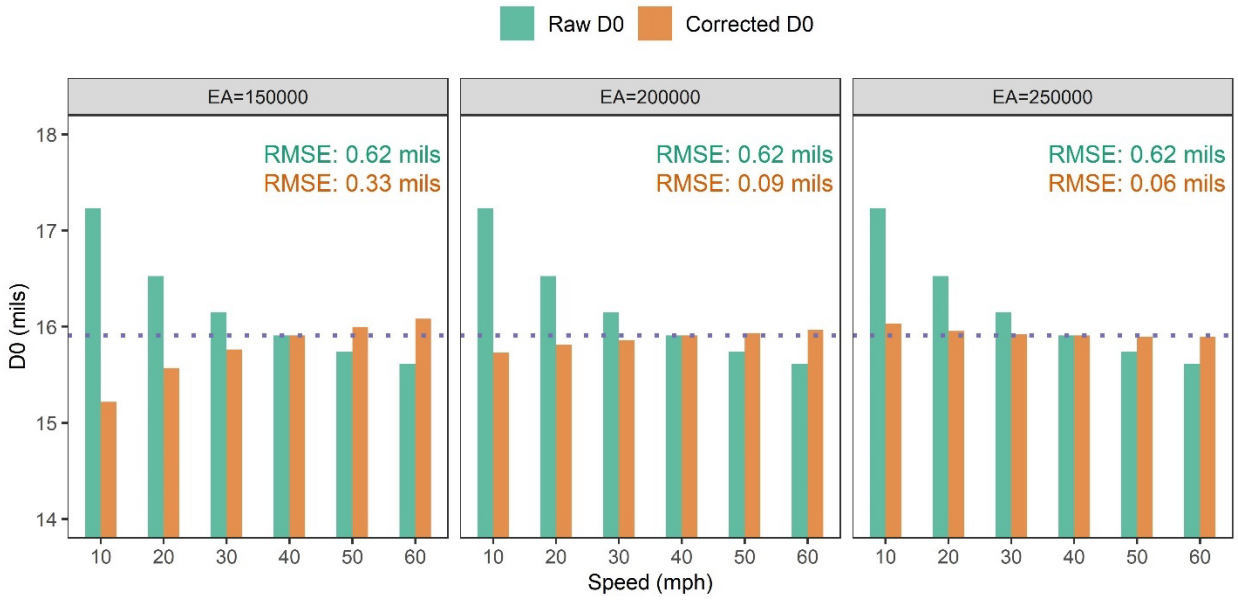

Figure 4-14. **Speed correction on D0**

The proposed speed correction method was applied to the theoretical D0 at different traffic speeds to verify its validity. The pavement structures and TSD deflections in **Figure 4-12** were used, and the effect of the estimation of ΔE_a on the speed correction was also explored. The difference between raw D0 and speed corrected D0 is shown in **Figure 4-14**. The test temperature was 20°C, which is equal to the reference temperature, so no temperature correction for TSD deflections was required. The reference speed was 40 mph, and D0 at a test speed of 40 mph is the reference D0, which is indicated by the dashed line in **Figure 4-14**. D0 at different speeds should be corrected to the reference D0, and the smaller the difference (RMSE), the better the correction. It was found that when the test speed was exactly equal to the reference speed (40 mph), the raw D0 is equal to the corrected D0. The effect of speed correction is related to the estimation of ΔE_a (actual ΔE_a is 215,900.1 J/mol for the AC material used in the simulation). The closer the estimated value of ΔE_a is to the actual ΔE_a, the better the speed correction will be. Overall, the RMSE of corrected D0 was always smaller than that of raw D0, so the corrected D0 is closer to the reference D0 than the raw D0.

4.3 Determining SN with TSD Deflections

The objective was to develop a new approach to determine the SN with TSD measurements by modifying the AASHTO method so that the improved TSD-based SN can be comparable to the existing FWD-based SN records. A general and reliable SN calibration method should apply to various pavement structures. However, a database of TSD deflections from a wide range of pavements is unavailable, and key pavement structure information (such as layer thickness) is often lacking in field data collection. Therefore, the numerical simulation method was preferred to obtain a universal and reliable calibration method.

A database of 243 different three-layer pavement structures was considered in terms of three levels of AC, base modulus, subgrade modulus, AC thickness, and base thicknesses, as presented in **Table 4-3**. The dynamic modulus curves of three plant-produced AC materials considered are presented in Appendices **Figure A-5** [38].

Table 4-3. Design factors in the parametric study

Levels	*Thickness (in.)*		*Modulus (ksi)*		
	AC	*Base*	*AC*	*Base*	*Subgrade*
Level 1	12	12	1500*	45	30
Level 2	8	9	1350*	30	15
Level 3	4	6	1100*	15	5

* Equivalent AC modulus corresponding to the equivalent loading frequency of FWD.

4.3.1 Simulation results and discussions

According to the simulation results of the parametric study, 243 deflection basin pairs for TSD and FWD data were obtained. To find out the underlying different mechanism of the AASHTO SN derived from the TSD and FWD, the deflection results under TSD and FWD testing should be compared. The deflection at the location x inches from the loading point was defined as Dx.

Figure 4-15 shows the deflection results comparison between TSD and FWD testing. There were many reasons for the different D0 (deflection at the loading center). For example, when other loading conditions were consistent, the different loading shapes of the TSD and FWD (dual circle versus single circle) would lead to a lower D0 for the TSD. The asymmetrical TSD deflection basin shape made the D0 lower than expected. The inertial damping and the AC viscoelasticity would result in a time difference between the time when the TSD crosses over the point and the time when the maximum response occurs, so D0 of the TSD was not the maximum deflection.

However, it can be found from **Figure 4-15**(a) that under the same contact pressure, the D0 for the TSD was always greater than the D0 for the FWD. In addition to the different loading radius of the TSD and FWD (equivalent to 6.72 inches vs. 5.904 inches, which would result in a greater D0 for the TSD but would not affect the back-calculation of the layer modulus), a more important reason was the different equivalent loading frequency of the FWD and TSD (16.7 Hz vs. 2.6Hz). Due to the rate-dependent viscoelastic nature of the AC layer, the AC layer exhibited lower stiffness under TSD testing than under FWD testing.

The surface curvature index (SCI) of the AC layer (SCI12, the difference between D0 and D12) is an important indicator of the strength of the AC layer. As shown in **Figure 4-15**(b), the SCI12 of the TSD was also greater than that of the FWD, which also indicated the lower stiffness of the AC layer under TSD testing.

The surface curvature index of the subgrade (SCI_subgrade, the difference between D36 and D60) reflects the strength of the subgrade. The different loading frequency (different equivalent AC modulus) of TSD and FWD testing also contributed to the SCI_subgrade difference. Compared to FWD, the AC layer tended to exhibit lower stiffness under the TSD (lower loading frequency); therefore, the subgrade was more heavily loaded and was expected to deform more. The results of SCI_subgrade confirmed this expectation, and the SCI_subgrade of the TSD was always greater than that of the FWD, as shown in **Figure 4-15**(c).

It should be noted that the equivalent loading frequency of the TSD was not assumed in the TSD simulation, and the viscoelasticity of the AC layer was represented by its dynamic modulus curve. The Fourier transform technology and frequency domain solutions adopted in 3D-Move enable the direct use of the frequency swept dynamic modulus in the analysis. A TSD-equivalent loading frequency description was only used to explain the underlying mechanism of different AC behavior under TSD and FWD tests.

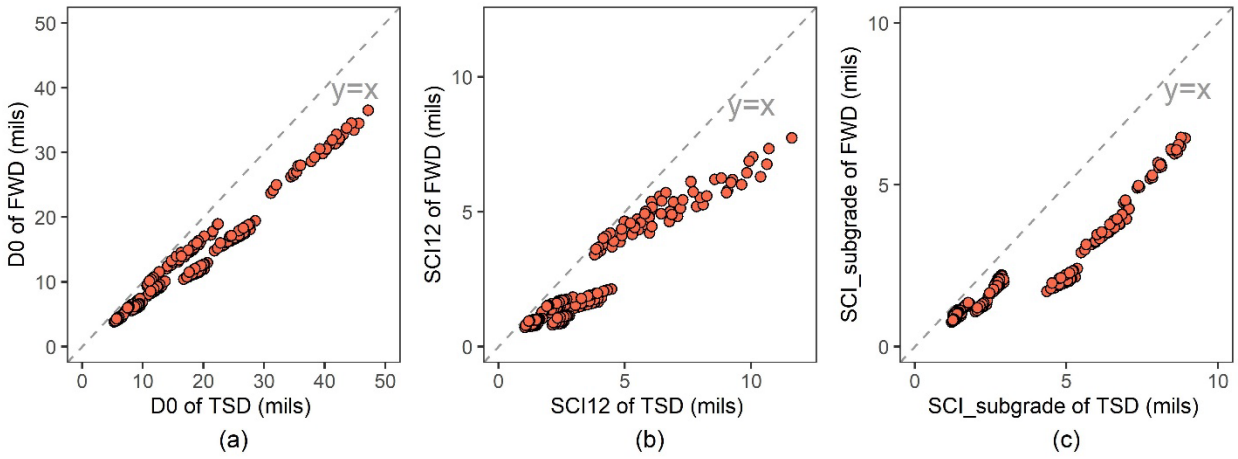

Figure 4-15. **Deflection comparison between TSD and FWD: (a) D0; (b) SCI12; (c) SCI_subgrade**

4.3.2 Sensitivity analysis

The influence of pavement structure variations on pavement deflections was also studied. An illustration of AC surface deflection basin for varying pavement structures is shown in **Figure 4-16**. The default AC material, base modulus, subgrade modulus, AC thickness, and base thickness were level 1, 30 ksi, 15 ksi, 8 inches, and 9 inches, respectively. Obviously, the greater the stiffness or thickness, the smaller the deflection, as weaker pavement structures would result in greater deflections. Deflections were more sensitive to subgrade modulus and AC thickness variations, but it was insensitive to the base layer. Therefore, both TSD and FWD deflections can be used to detect weak asphalt layers and weak subgrade, but they were not effective in detecting the damage in the base layer.

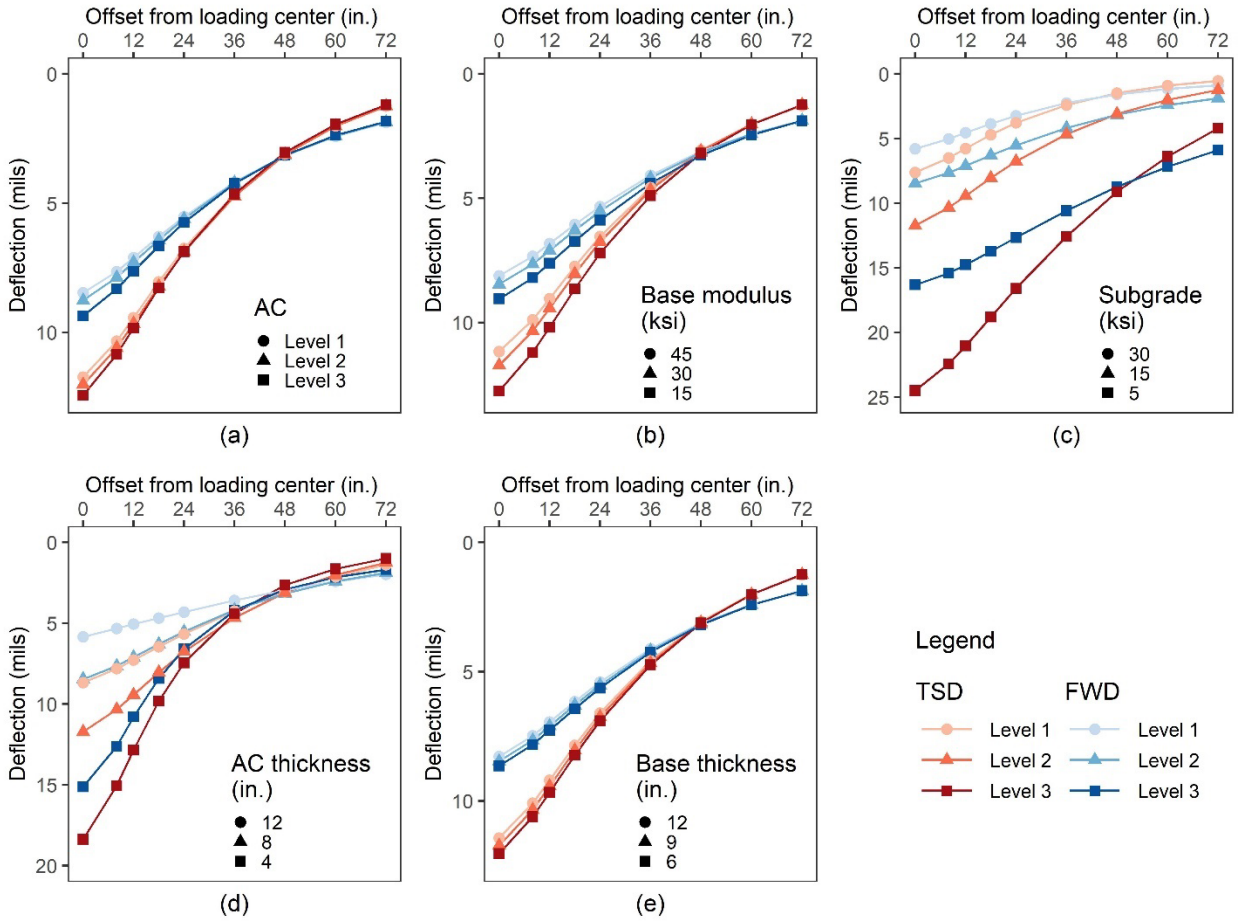

Figure 4-16. **3D-Move deflections for varying pavement conditions: (a) AC dynamic modulus; (b) base modulus; (c) subgrade modulus; (d) AC thickness; (e) base thickness**

The deflection at locations close to the loading center were more sensitive to different pavement structural factors while the deflection at locations far from the loading center were almost exclusively related to the subgrade modulus. It confirmed the assumption in the AASHTO back-calculation procedure that at a location sufficiently far from the loading center, the deflection of the AC surface (the cumulative deformation of all layers) was almost entirely due to deformation in the subgrade. Overall, the sensitivity of FWD deflections and TSD deflections to different pavement structural factors was almost the same.

In addition to the deflection itself, the deflection basin shape can also provide some useful information. At locations close to the loading center, the deflection of the TSD was greater than that of the FWD, while the opposite occurred at locations far from the loading center. As a result, the deflection basins of the TSD were steeper than those of the FWD, and they crossed each other at about 48 inches from the loading center. The deflection basin shape depended on the stress distribution among different layers. Assuming a series of pavement structures with the same subgrade modulus and upper layer thicknesses but different upper layer stiffness, the structure with the softer upper layer would have narrower vertical stress distribution and a steeper basin if the same load is applied to each structure. In contrast, structures with stiffer upper layers have

flatter deflection basins. Therefore, the steeper basin shape of the TSD also came from the relatively lower loading frequency of the TSD (lower stiffness of the AC layer under it).

4.3.3 AASHTO back-calculation analysis

After obtaining the 243 theoretical TSD and FWD deflection basin pairs, the back-calculation analysis was performed on each deflection pair according to the 1993 AASHTO Pavement Design Guide. The subgrade radius, subgrade resilient modulus (AASHTO M_r), and effective pavement modulus (AASHTO E_p) for different pavement structures derived from TSD and FWD testing can be obtained, respectively.

Subgrade radius is defined as the radial distance of the deflection used for subgrade resilient modulus calculation in Equation (3-4). In the engineering practice of deflection collections, deflections are typically recorded at the following locations: 0, 12, 18, 24, 36, 48, and 60 inches from the loading center. Therefore, the subgrade radius should be selected from these specific locations (generally starting at 24”). The detailed process of SN calculation is as follows:

Step 1: Input the layer thickness, deflection, and its position (offset). Set the subgrade radius to 24 inches.

Step 2: Calculate the subgrade resilient modulus based on the deflection at the subgrade radius using Equation (3-4).

Step 3: Calculate the effective pavement modulus based on D0 and the subgrade resilient modulus (calculated in Step 2) using Equation (3-5).

Step 4: Check whether the subgrade radius meets the requirements of Equation (3-6) and (3-7). If yes, stop; otherwise, go to Step 5.

Step 5: Update the subgrade radius to a greater one (among 24”, 36”, 48”, and 60”), then go to Step 2.

4.3.3.1 Subgrade radius

Figure 4-17(a) compares the subgrade radius of the TSD and FWD of different pavement structures. It can be found that there are four different FWD subgrade radii (24”, 36”, 48” and 60”) and three different TSD subgrade radii (24”, 36” and 48”) for these 243 pavement structures. When the TSD subgrade radius is 24 inches, the FWD subgrade radius can be 24 inches or 36 inches. When the TSD subgrade radius is 36 inches, the FWD subgrade radius can be 36 inches, 48 inches, or 60 inches. Similarly, when the TSD subgrade radius is 48 inches, the FWD subgrade radius can be 48 inches or 60 inches. Therefore, the subgrade radius of the TSD is generally less than or equal to the subgrade radius of the FWD. It is assumed that starting from the subgrade radius, the deformation almost only causes the surface deflection in the subgrade and is independent of other pavement layers. Therefore, the vertical stresses in the pavement layers (above the subgrade) tend to be distributed over a narrower area under TSD loading than FWD, indicating a steeper deflection basin of the TSD.

4.3.3.2 Subgrade resilient modulus

The subgrade resilient modulus calculated using TSD deflections and FWD deflections is shown in **Figure 4-17**(b), which is colored by the assumed value in the simulation. It can be found that the AASHTO subgrade resilient modulus calculated using TSD deflections is always greater than

that calculated using FWD deflections (RMSE was 3.04 ksi), and the difference increases with the increase of subgrade modulus. For pavements with stiff subgrades (subgrade modulus greater than 30 ksi), the subgrade resilient modulus back-calculated using FWD deflections is smaller than the subgrade modulus assumed in the 3D-Move simulation, so the back-calculation analysis based on FWD deflections tends to underestimate the stiff subgrade. For pavements with soft subgrades (subgrade modulus less than 5 ksi), the subgrade resilient modulus calculated by deflections is greater than the assumed value, so the AASHTO back-calculation analysis tends to overestimate the soft subgrade. Overall, the subgrade resilient modulus calculated from theoretical deflections (both FWD and TSD) is close to the subgrade modulus assumed in the 3D-Move simulation, so the AASHTO subgrade resilient modulus derived from FWD and TSD deflections are both good estimates of the actual subgrade modulus.

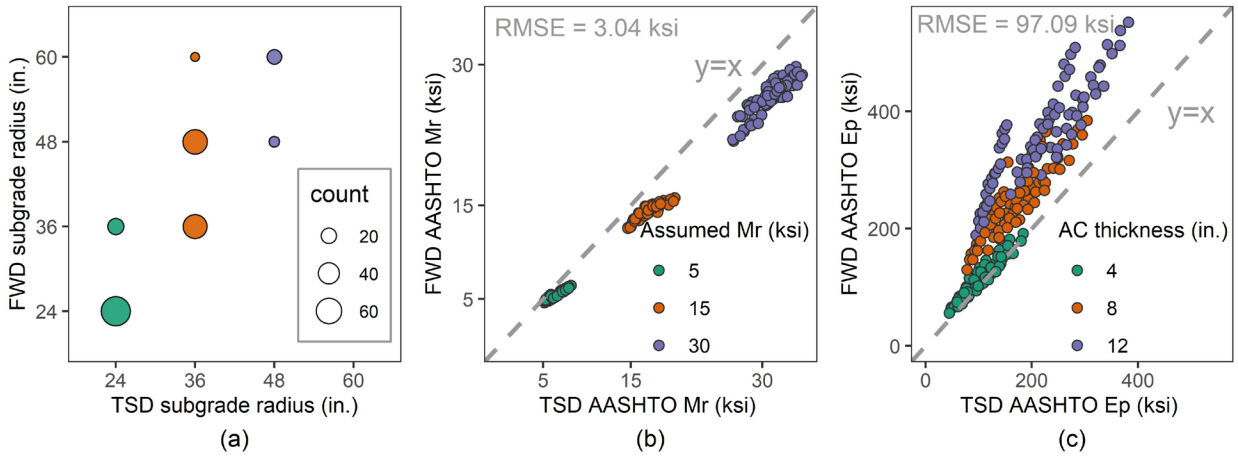

Figure 4-17. **AASHTO SN calculation process: (a) AASHTO subgrade radius; (b) AASHTO subgrade resilient modulus; (c) AASHTO pavement effective modulus**

4.3.3.3 Effective pavement modulus

The effective pavement modulus represents the overall strength of pavement layers above the subgrade, and it is a composite modulus that depends mainly on the stiffness of the AC layer and the thickness of the AC layer. It has been shown that AC layers tend to exhibit lower stiffness at TSD (lower loading frequency), so the effective pavement modulus is expected to be smaller for TSD than for FWD. As shown in **Figure 4-17**(c), the AASHTO effective pavement modulus calculated using TSD deflections was generally smaller than that calculated using FWD deflections (RMSE was 97.09 ksi), and the difference increased with the increase of AC thickness. When the AC thickness was 4 inches, the effective pavement modulus calculated from TSD and FWD deflection was similar. This is because when the AC thickness is small, the smaller equivalent AC modulus under the TSD is offset by the effects of dual circular loading and asymmetric basins of TSD. As described in Section 4.3.2, the dual circular loading shape and asymmetric basin of the TSD make the D0 of the TSD lower than expected, which may result in a greater than expected effective pavement modulus (back-calculated from D0).

4.3.4 TSD-based SN calibration

The AASHTO SN calculated from the theoretical TSD and FWD deflections according to the AASHTO procedure is shown in **Figure 4-18**(a). Similarly, it can be found that for most of the

pavement structures, the AASHTO SN calculated using FWD deflection is larger than the SN calculated using TSD deflection except for some cases where the AC thickness was 4 inches. Furthermore, the difference in SN between TSDs and FWDs increases with the increase in AC thickness. The difference between the two (RMSE) is about 0.74, which means that the TSD-based AASHTO SN is expected to be 0.74 lower than the FWD-based AASHTO SN. In pavement rehabilitation and overlay design, the difference in effective SN estimates could result in a 1.85-inch difference in AC thickness (Equation (4-2)).

$$D_{ol} = \frac{SN_{ol}}{a_{ol}} \tag{4-2}$$

where SN_{ol} is the required overlay structural number, a_{ol} is the structural coefficient for the AC overlay (0.4), D_{ol} is the required thickness of AC overlay (inches).

4.3.4.1 Linear regression

The existing SN records in the PMS are based on FWD deflections, and the TSD-based AASHTO SN needs to be calibrated to compare with the FWD-based values. A linear regression was performed on the TSD-based AASHTO SN to make it closer to the FWD-based AASHTO SN, which has the following form:

$$SN_{linear} = 1.22 * SN_{tsd} - 0.33 \tag{4-3}$$

where SN_{tsd} is TSD-based AASHTO SN and SN_{linear} is the TSD-based SN improved by linear regression. It (RMSE of 0.33) is more accurate than the direct application of the AASHTO procedure, but there is still room for improvement.

4.3.4.2 Calibration by AC thickness

Since the simple linear regression could not eliminate the difference between the FWD-based SN and TSD-based SN, more complex regression methods or the introduction of other variables were required. Therefore, a machine learning method, Random Forests (RF), was employed to evaluate which factor was most important for predicting FWD-based AASHTO SN [39]. RF works by constructing a large number of decision trees during training and outputting them as class patterns (classification) or mean prediction (regression). As a tree-based learning algorithm, it is convenient to interpret RF models through variable importance information, which describes the relative contribution of the input variables to the prediction.

The RF model was established using the FWD-based AASHTO SN as the response variable. The influencing factors involved in the AASHTO SN calculation procedure, combined with the TSD-based AASHTO SN, were used to predict the RF model. Considering that the base layer thickness is less available than the AC thickness in the network-level application, the pavement thickness is divided into the AC thickness and the base layer thickness (both of which are used as predictors). **Figure 4-18**(b) shows the importance ranking of different predictors. It can be found that the TSD-based AASHTO SN is the most important factor in predicting the FWD-based AASHTO SN. AC thickness also contributes significantly, while other factors have little effect.

For the sake of simplicity, only the most important factors were included in the calibration of the TSD-based SN. Therefore, taking into account the effect of AC thickness, the following form can be obtained:

$$SN_{ac} = 0.81 * SN_{tsd} + 0.19 * H_{ac} - 0.15 \tag{4-4}$$

where SN_{tsd} is TSD-based AASHTO SN, H_{ac} is the thickness of the AC layer, and SN_{ac} is the TSD-based SN calibrated by H_{ac}. The calibration effect of AC thickness on the TSD-based SN is shown in **Figure 4-18**(c). It can be found that the difference between the SN calculated from TSD and FWD deflections has been corrected sufficiently, and the RMSE between them is 0.17, which is more accurate than the linear regression.

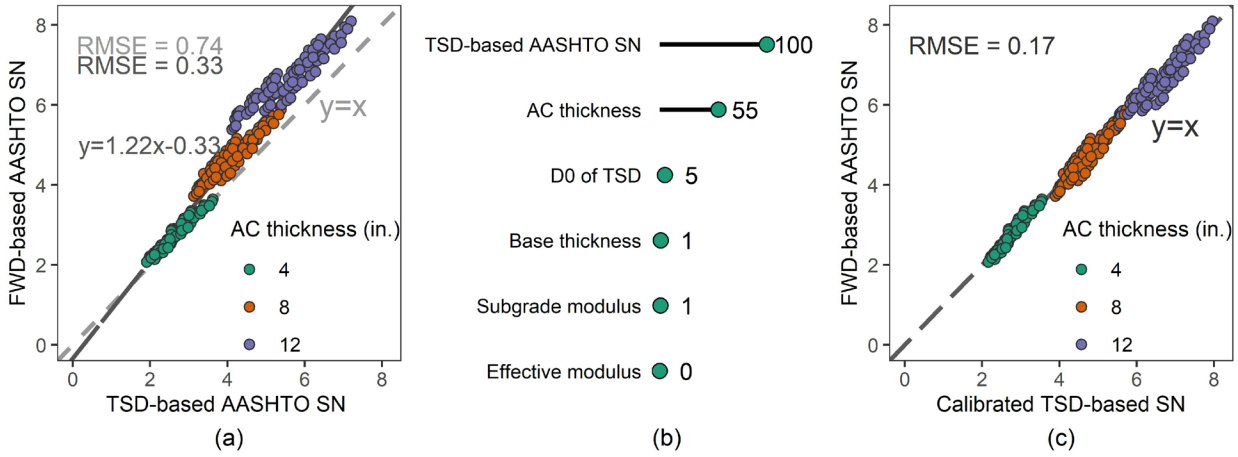

Figure 4-18. **TSD-based SN: (a) Linear regression; (b) Variable importance of the random forest model; (c) Calibration by AC thickness**

The testing RMSE of the RF model is also 0.17. Since the RF model is too complex for engineering applications, the RF model in this study is only used as a reference to evaluate the accuracy of other methods. The accuracy of the TSD-based SN calibrated by AC thickness is very close to that of the RF model, so it is considered to be sufficiently accurate without further improvement.

In summary, the direct application of the AASHTO method to calculate the SN with TSD deflections had a relatively large RMSE of 0.74, while the TSD-based SN improved by linear regression made great progress. The most accurate method for estimating the SN with TSD deflections was the SN calibrated by the AC thickness, with the smallest RMSE of 0.17. Moreover, it was able to achieve the same accuracy as the much more complicated RF method, so it can be considered sufficiently accurate in terms of its simplicity.

4.4 Correlation Analysis Between Deflection Lag and Fatigue Cracking

4.4.1 Phase angle and AC fatigue

It has been proven that the phase angle of the AC material increases gradually with the loading cycles as the AC is repeatedly loaded. When the sample starts to break down, the phase angle reaches its maximum value and then begins to drop rapidly. The same conclusion can be extended to the actual pavement. The newly constructed AC layer will have the smallest phase angle, and the phase angle will be significantly different between pavements with and without fatigue cracking. The phase angle gradually approaches its maximum value as the fatigue crack increases. After this point, the pavement will suffer severe fatigue damage. Therefore, if the phase angle can be measured during the pavement service life, the current and impending pavement conditions can be effectively assessed and predicted.

However, estimating the phase angle of existing AC layers from drilled core samples is destructive, expensive, and not necessarily suitable for large-scale applications. Therefore, the relationship between the lag in the TSD deflection basin and phase angle was investigated, and the possibility of estimating pavement conditions from the TSD deflection lag was evaluated.

The relationship between the lag in the TSD deflection basin and AC fatigue (phase angle) was evaluated by simulating the pavement responses with different AC phase angles under TSD loading using the 3D-Move program. A three-layer pavement structure was assumed, as shown in **Table 4-1**. The phase angle of the AC layer was represented by the damping ratio, and the relationship between the phase angle (Φ) and damping ratio (ξ_{AC}) is given by:

$$\zeta_{AC} = 0.5\tan(\varphi) \tag{4-5}$$

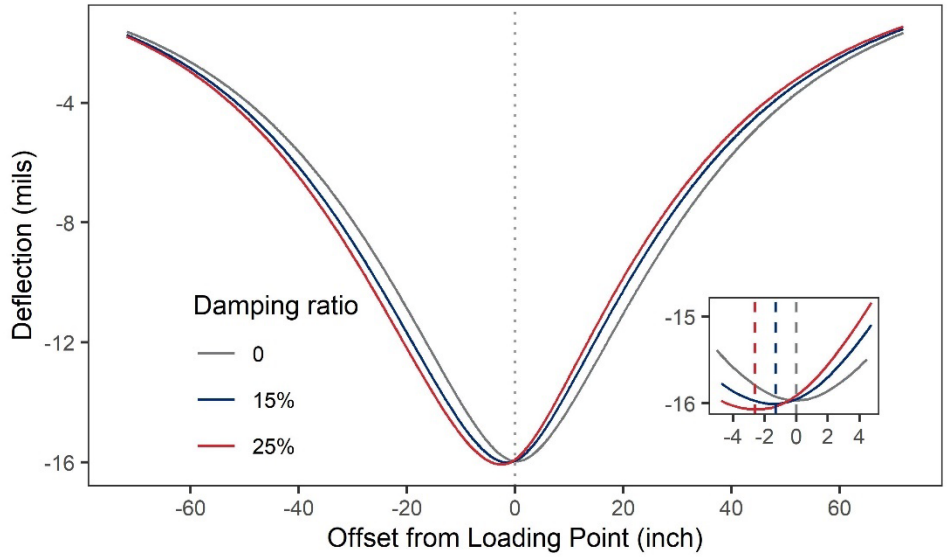

Figure 4-19. **The influence of AC damping ratio on deflection lag**

Three levels of fatigued AC layers with damping ratios of 0, 15%, and 25% were considered, corresponding to phase angles of 0, 17, and 28 degrees. As shown in **Figure 4-19**, the TSD deflection basin is almost symmetric when the damping ratio of the AC layer is zero. As the damping ratio increases, the deflection lag distance also increases. Therefore, the lag distance increases with increasing fatigue levels, and the TSD deflection lag can be used as an indicator of the fatigue condition of the AC layer. When the phase angle increases by 10 degrees, the TSD lag distance increases by about one inch.

4.4.2 Influencing factors of lag distance

In addition to the phase angle of the AC layer, there are other factors that may affect the lag distance of the TSD deflection basin and thus interfere with the detection of fatigued AC layers. The pavement responses under the TSD depends on pavement structures, and different pavement structures may have different lag distance. In addition, the viscoelasticity of the AC layer is related to the temperature and loading frequency (TSD speed). Due to the time-temperature equivalence principle, i.e., the effects of loading frequency and temperature on AC

viscoelasticity are equivalent, only the effect of loading frequency (TSD speed) on the lag distance was investigated.

4.4.2.1 TSD speed

The sensitivity of the lag distance to TSD speed was evaluated by considering six levels of TSD speed, as presented in **Table 4-4**. Simulations were based on the three-layer pavement structure presented in **Table 4-1**, where the modulus and phase angle of the AC layer were both rate-dependent. The theoretical lag distance was calculated from 3D-Move simulation results, which will be discussed later. For normal TSD speeds (10-60 mph), a greater speed (loading frequency) usually corresponds to a greater phase angle of the AC layer and, therefore, a larger lag distance. However, for different TSD speeds, the lag distance does not differ much, and the lag distance is insensitive to TSD speeds.

Table 4-4. The sensitivity of the lag distance to TSD speed

TSD speed (mph)	*10*	*20*	*30*	*40*	*50*	*60*
Lag distance (inch)	1.44	1.46	1.48	1.50	1.51	1.53

4.4.2.2 Pavement structure

Due to the lack of pavement structure information combined with field TSD deflection data, the theoretical database of TSD deflections containing various pavement structures was developed through the 3D-Move program, as listed in **Table 4-3**. In order to exclude the effect of the phase angle of the AC layer, the AC damping ratio was set to an identical constant of 25% for all pavement structures.

The 3D-Move simulation results show different pavement structures showing different lag distances even at the same AC phase angle. The importance ranking of different pavement parameters on the lag distance was obtained based on the random forest (RF) method, as shown in **Figure 4-20**(a). The AC thickness is the important factor affecting the lag distance, and subgrade modulus also contributes significantly. The effect of types of plant-produced AC materials, the modulus, and thickness of the base layer is negligible.

Figure 4-20(b) shows the effect of AC thickness and subgrade modulus on the lag distance. With the increase of AC thickness, the TSD lag distance increases. In addition, a weaker subgrade will result in a greater lag distance. Therefore, the lag distance is related to the pavement structure, and the lag distances of pavements with different structures cannot be directly compared to identify the fatigue sections. It may be possible for the same road section (with the same pavement structure) to identify the fatigued section by comparing the lag distance.

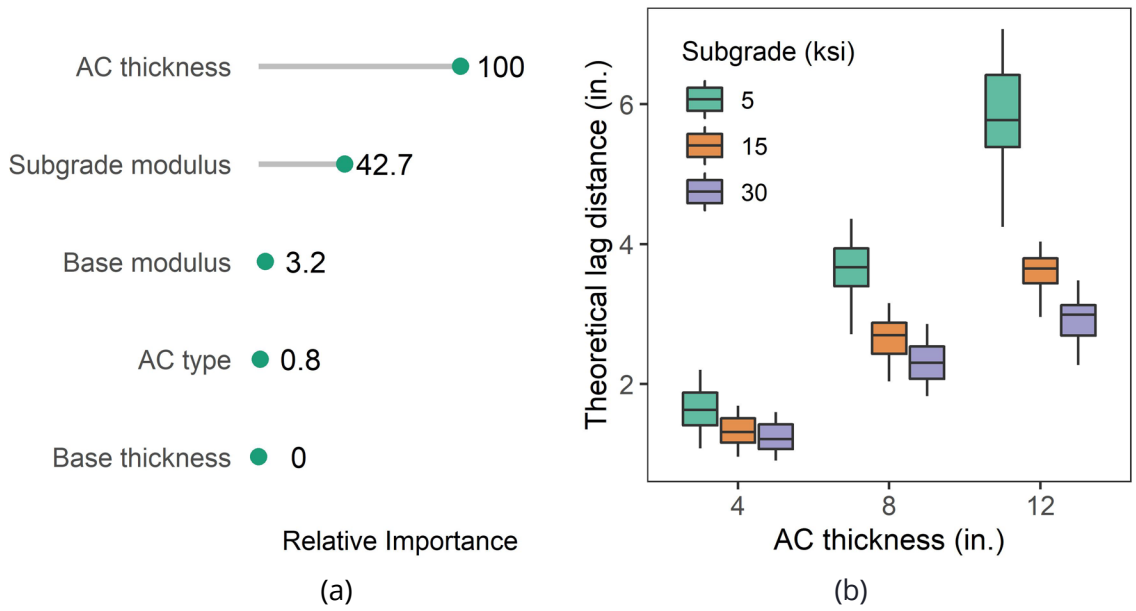

Figure 4-20. **The influence of pavement structures on lag distances**

4.4.3 Field lag distance evaluation

4.4.3.1 Lag calculation method evaluation

The accuracy and feasibility of different lag calculation methods were evaluated using 3D-Move simulation results for 243 pavement structures, listed in **Table 4-3**. The fitted lag distance was calculated from ten TSD slopes located at -18, -12, -8, 5, 8, 12, 18, 24, 36, and 60 inches from the loading center. The theoretical lag distance was also calculated by fitting the TSD slope curve by the Makima method but using a finer point spacing of 0.26 inches (a total of 1024 TSD slope points), which is the output spacing of the 3D-Move program.

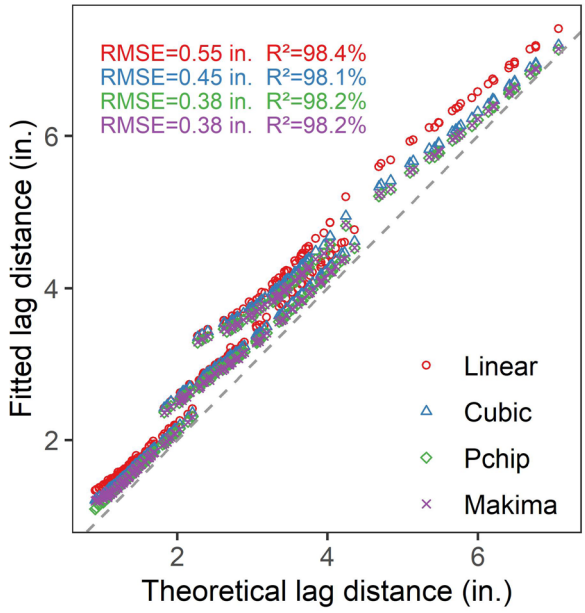

Figure 4-21. **Comparison of four interpolation methods**

Figure 4-21 shows that the fitted lag distance calculated by different interpolation methods is similar. The Pchip and Makima interpolation ties for the best with the smallest RMSE (0.38 inches), which means that the fitted lag distance is expected to deviate from its theoretical value by 0.38 inches. Compared with other methods, linear interpolation tends to yield higher fitted lag distances, especially when the lag distance is greater than 5 inches. The linear interpolation has the largest RMSE while the smallest R-squared (R^2). Although there are errors in the fitted lag distance, the ranking of the fitting results is almost the same as the ranking of the theoretical value. Considering the simplicity of linear interpolation, it is considered sufficiently accurate and practical to provide at least an initial guess about the lag distance at the network-level.

4.4.3.2 Field lag distance evaluation

The TSD slope curve fitting method was applied to field TSD slope measurements collected from in-service pavements in Tennessee to calculate lag distances of various pavement conditions. Since interpolation forces the curve to pass through all data points, it cannot exclude or filter out abnormal slope measurements. The Linear interpolation is only relevant for the two slope measurements located near the loading center (which is critical for all interpolation methods), while other interpolation methods are sensitive to all abnormal slope measurements. Therefore, the linear interpolation method was adopted in the lag distance calculation at the network-level. In addition to the interpolation error, the testing error of the TSD device should not be ignored, especially when the TSD slope measurement is small. In some cases, the fitted lag distance can even be negative, which means that the calculated zero-slope point falls in front of the loading point. Therefore, the related data were excluded for pavement sections with small TSD slopes (S5 <= 100 μm/m).

The fatigue cracks area is usually used to reflect the fatigue condition of the pavement, and it can be divided into different levels to reflect the different stages of fatigue cracks development. Wang et al. considered 3.6% as the cut-off point between the slow and rapid growth of fatigue cracking [40]. The FHWA defines pavements with less than 5% fatigue cracks as good condition and pavements with greater than 20% fatigue cracks as poor condition [41]. In this study, pavement fatigue conditions were classified into four levels corresponding to the fatigue crack development stages of no cracks (0), early (0-5%), intermediate (5%-20%), and late (>20%).

Figure 4-22 shows the relationship between TSD lag distance and fatigue cracking. It can be found that the fitted lag distance was the smallest for pavements without fatigue cracks. The lag distance increases gradually with increasing fatigue crack area (early stage) and reaches a peak at the intermediate stage of the crack development (5%-15%). Thereafter, the lag distance decreases with the increase in fatigue crack area until fatigue failure occurs (late stage). Notice that the lag distance shows the same pattern as the phase angle under repeated loading (**Figure 2-4**). The four pavement fatigue levels, no crack, early, intermediate, and late, can be associated with the four characteristic regions in the phase angle, corresponding to the internal heating, micro-crack formation, crack formation, and breakdown, respectively.

However, due to the numerous factors affecting the TSD lag distance, the lag distance within each fatigue level varies greatly. In addition, there is a large overlap in the lag distances of different fatigue levels. It has been shown that the pavement structure has a significant effect on the lag distance, so different pavement sections with unknown structures cannot be compared directly. The lag distances were compared for different sections on the same route (assuming the same

pavement structure). As shown in **Figure 4-23**, for some route sections in Tennessee, the fatigue crack area is closely related to the lag distance. Although there are occasional differences, in general, the lag distance and fatigue crack area always follow the same trend.

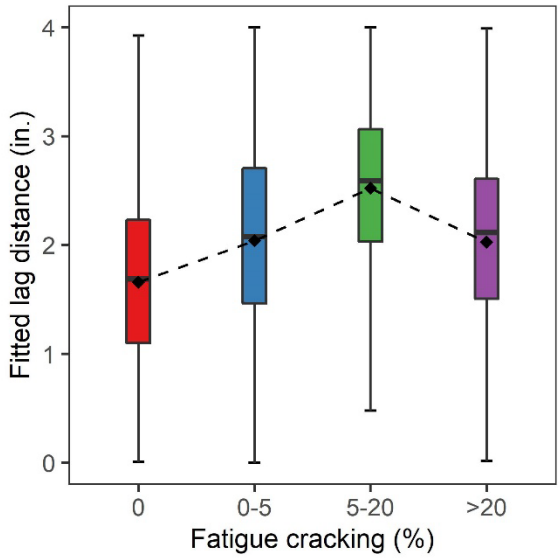

Figure 4-22. **Relationship between TSD lag distance and fatigue cracking**

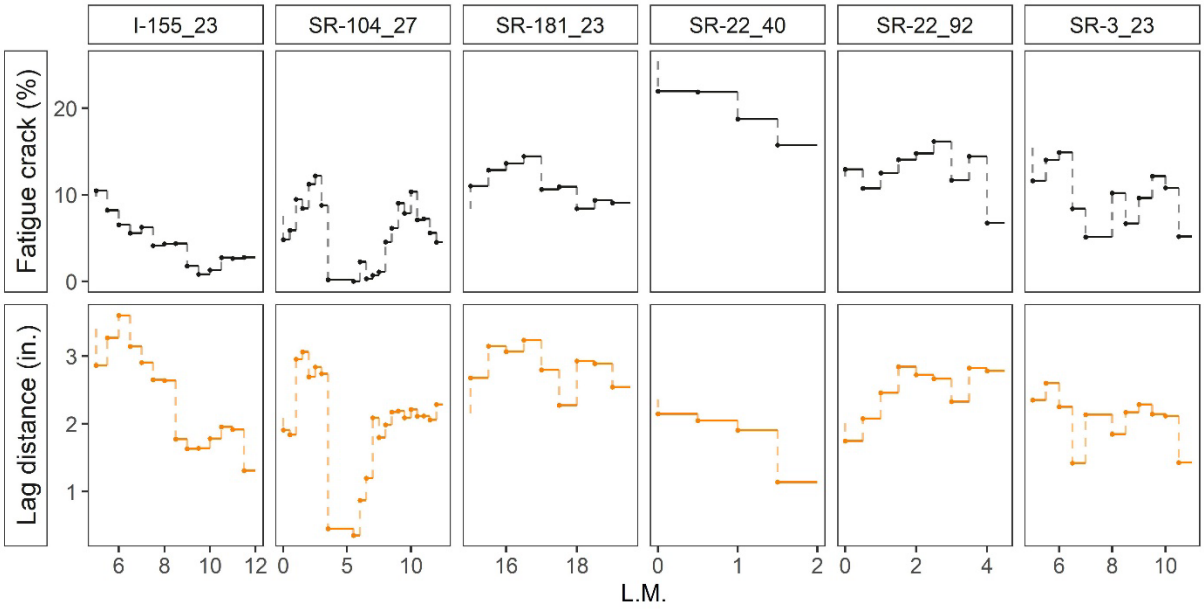

Figure 4-23. **Lag distance for cracked pavements**

The area of fatigue cracking does not always coincide with the lag distance. This can be explained by the fact that fatigue cracks are an explicit indicator of the pavement fatigue level, while the lag distance implicitly indicates the fatigue condition of the pavement. Some sections show only a small amount of fatigue cracks, but with a large lag distance. In this case, it can be assumed that fatigue distress has already occurred in the AC material and more fatigue cracks can be expected to appear soon. In **Figure 4-24**, road SR-457-27 shows a small amount of fatigue cracks (less than

5%), and the larger the lag distance, the more fatigue cracks there are. Similarly, on SR-372_92, fatigue cracking seems to follow the trend of lag distance, i.e., a few cracks start to appear at locations with relatively large lag distances. It can be inferred that the lag distance can be used to predict the initiation and growth of fatigue cracks. For pavements that are currently crack-free (SR-183_66, SR-366_27, SR-5_57), fatigue cracks are expected to initiate at locations with relatively large lag distances.

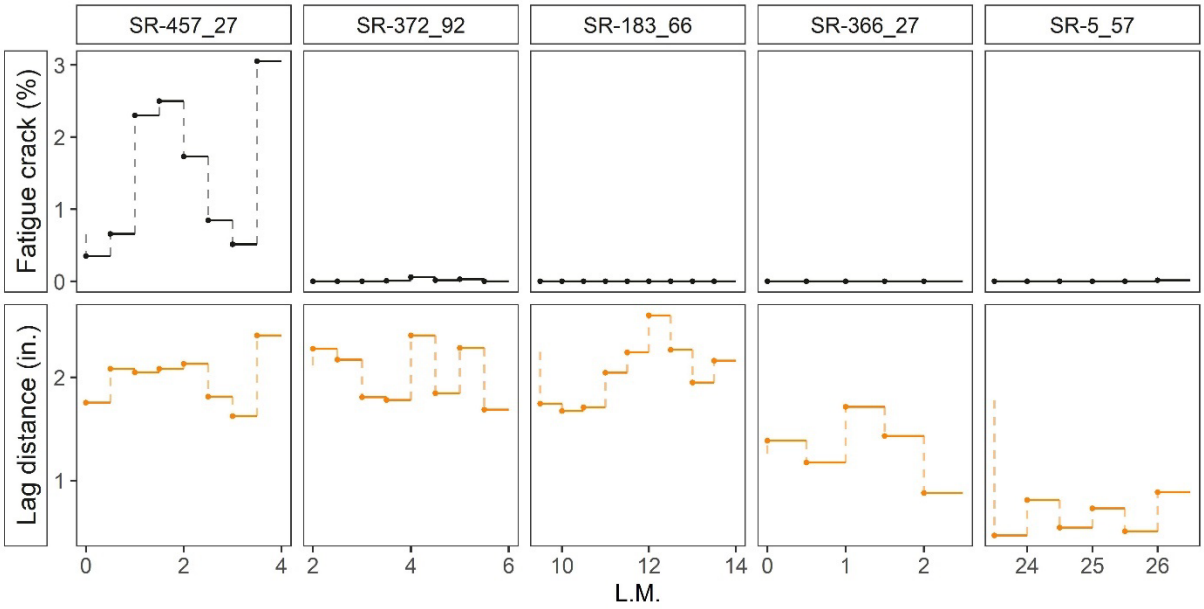

Figure 4-24. **Lag distance for crack-free pavements**

4.5 Incorporating TSD Data Within PMS

4.5.1 Correlation between TSD and pavement performance

Figure 4-25 shows the D0 and pavement performance for all TSD route sections. There were, in total, 86 valid TSD route sections, which were ranked by their median D0. D0 is the overall strength index of the entire pavement structure; the higher the D0, the lower the structural capacity. For the sections with higher D0, the pavement performance is expected to be poorer. However, some sections with high D0 perform poorly, but for most sections, there was no significant correlation between pavement performance and D0. Sections with high D0 tend to show greater IRI and more fatigue cracking while there are still some sections with high D0 but lower IRI and less fatigue cracking, or vice versa. The pavement rutting appears to be rather random and does not show any correlation with D0.

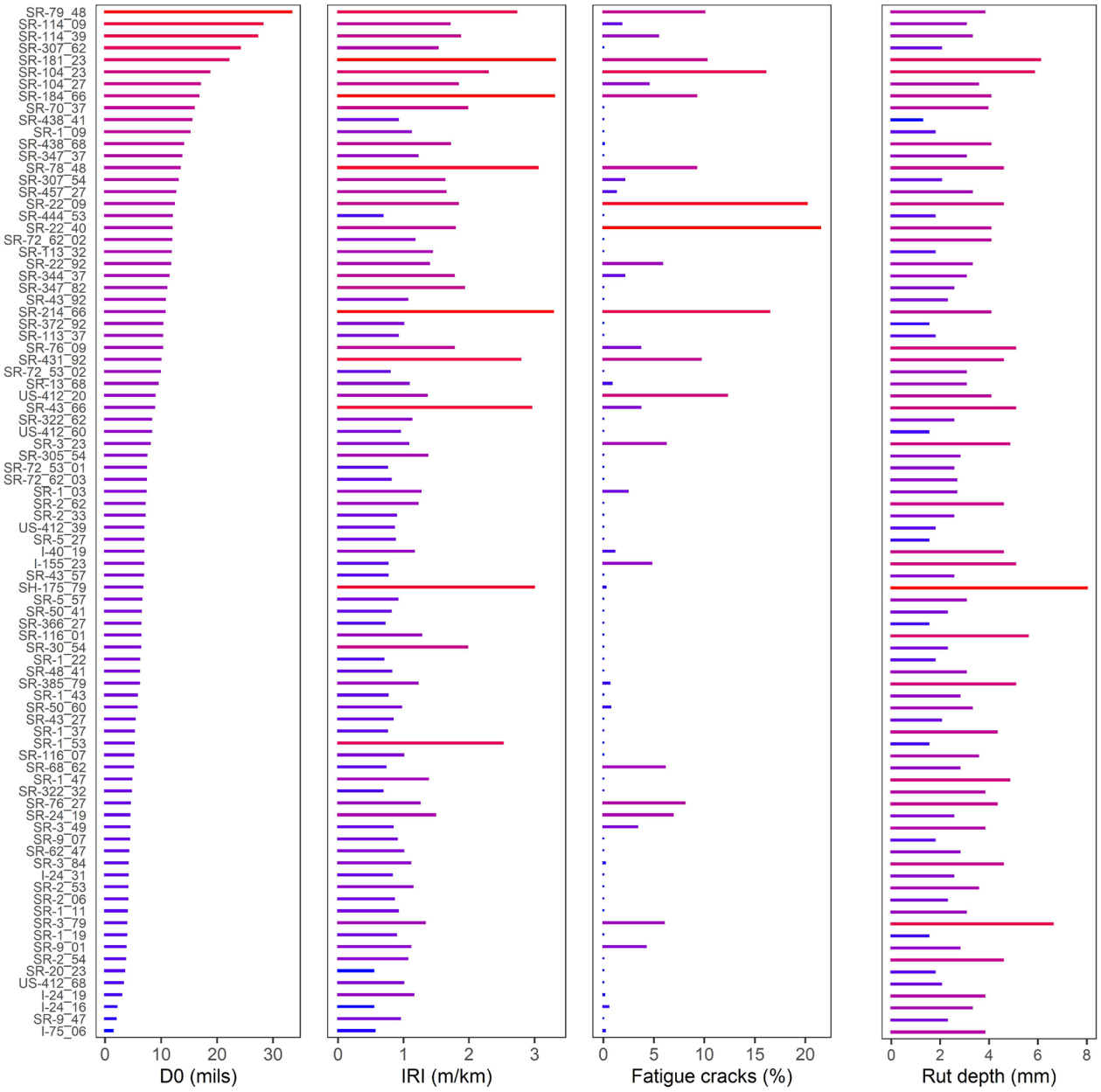

Figure 4-25. **D0 and pavement performance for all TSD route sections**

Table 4-5 shows the Spearman rank correlation between the TSD deformation index and the pavement performance index. The Spearman correlation measures the statistical dependence between the ranks of two variables (rank correlation). It will be high when the ranks of the two variables are similar (or identical for a correlation of 1) and low when the ranks of the two variables are dissimilar (or exactly the opposite for a correlation of -1). It can be found that the Spearman correlation between D0 and IRI is the largest, but only 0.13. The correlations for all other combinations are less than 0.1, indicating that the rank correlation between deflections and pavement performance is negligible. This means that pavement performance indicators do

not adequately reflect the pavement structural condition and that the role of deflection measurements cannot be replaced.

Table 4-5. Rank correlation between TSD and pavement performance

Index	*IRI*	*Gator cracking*	*Rutting*
D0	0.13	0.02	0.00
SCI_12	0.09	0.01	0.00
D60	0.08	0.06	0.02

4.5.2 Structural condition evaluation

Deflection measurements have a wide range of applications in structural evaluation and are often used in combination with layer thickness. The 1993 AASHTO design guide introduced a method to estimate the SN of existing pavement based on FWD deflection and layer thickness. As discussed in Section 4.3, the existing pavement structural strength can be estimated by the effective SN. The structural strength index (SSI) is defined as the ratio of the effective SN (SN_{eff}) to the required SN (SN_{req}) of the pavement [43].

$$SSI = \frac{SN_{eff}}{SN_{req}} \tag{4-6}$$

Based on design charts in the 1993 AASHTO Pavement Design Guide, the required SN can be calculated from the subgrade modulus and the estimated equivalent single axle loads (ESALs) for the next 20 years. An SSI equal to or greater than 1 indicates that the pavement structural condition is sufficient for the estimated future ESALs. However, when the SSI is less than 1, M&R should be considered to improve the structural capacity of the pavement. **Table 4-6** lists the SSI threshold values for different M&R intensities [43].

Table 4-6. Structural strength index threshold values.

SSI	*Treatment intensity*
> 90%	Do Nothing
80%-89%	Preventative maintenance
65%-79%	Light rehabilitation
50%-64%	Medium rehabilitation
0-49%	Heavy rehabilitation

Combined with layer thickness, deflection can also be used to back-calculate the layer modulus. However, the layer thickness is often lacking in the early stages of pavement evaluation and may vary considerably over the length of the pavement, which affects the effectiveness of pavement structural evaluation. Therefore, a benchmark method based on deflection measurements has been developed, namely Deflection Bowl Parameters (DBPs). It provides a simple and quick way to make a preliminary estimate of pavement structural conditions without the need for layer thickness [43]. DBPs estimate the pavement structural condition by deflection indices based on their strong relationship with the layer strength. It should be noted that SSI can be used to identify weak sections, but not the root cause of pavement structural weakness. However, DBPs can be used to identify not only weak sections but also weak layers, thus helping to identify the actual source of structural weakness in the pavement.

It has been mentioned in Section 4.3.2 that the deflection is effective in detecting weak asphalt layers and weak subgrade but is not sensitive to the weakness of the granular base layer. The SCI_12 and D60 are used to represent the strength of the AC layer and subgrade in the proposed DBPs system. The recommended benchmarks (not yet calibrated by TDOT) for pavement condition assessment are presented in **Table 4-7**, and the thresholds were estimated based on the Texas reference values (See Appendices **Figure A-6**) [43]. The thresholds for SCI_12 are different for different route types, while the D60 is the same. The thresholds should be developed empirically and then calibrated by local data. However, the current TSD dataset is relatively small and biased, so the thresholds presented in **Table 4-7** are not locally calibrated.

The threshold of pavement quality index (PQI) is defined based on the Tennessee criteria. The fair condition indicates that the pavement needs to be observed and monitored for further improvement. The poor condition indicates a high-priority occurrence that needs to be addressed as soon as possible to maintain the pavement soundness. The Texas structural condition benchmark is based on a contact pressure of 82.2 psi for the FWD deflection, so all TSD deflections should be corrected to the same contact pressure (82.2 psi) before the benchmark analysis is performed.

Table 4-7. Pavement condition assessment benchmark

	Index	*Interstates*	*State Routes*	*Evaluation*
Structural	SCI_12	<6	<10	Good AC
		6-10	10-20	Fair AC
		>10	>20	Poor AC
	D60	<1	<1	Good Subgrade
		1-2.2	1-2.2	Fair Subgrade
		>2.2	>2.2	Poor Subgrade
Functional	PQI	>4	>3.5	Good Performance
		2-4	2-3.5	Fair Performance
		<2	<2	Poor Performance

4.5.3 Incorporating TSD within PMS (PMS & DBPs)

The well-known RAG condition rating system, which is often applied in PMS and pavement condition ratings, was used in the TSD routes assessment. The TSD routes were assessed on a one-mile segment basis (median value of each index per mile segment). In the traditional RAG, red represents severe condition (Address), amber represents warning condition (Monitor), and green represents good condition (Do nothing). **Table 4-8** shows the TSD route assessment results based on PMS (PQI) only.

In conjunction with the DBPs classification, the severe condition is divided into four subcategories: purple (preventative maintenance), pink (light rehabilitation), magenta (medium rehabilitation), and red (heavy rehabilitation or reconstruction). **Table 4-9** shows the TSD route assessment results based on PMS+DBPs. It can be found that 57.14% of interstates and 67.72% of state routes are in the good (or fair) condition in terms of functional performance and structural capacity. There are 2.38% of interstates and 2.05% of state routes with satisfactory structural capacity at both AC layer and subgrade, despite poor functional condition (poor PQI).

In this case, light rehabilitation (e.g., sealing) is sufficient, and no further expenditure is required. There are 7.65% of state routes that show unsatisfactory functional conditions because of the insufficient structural capacity of the subgrade. The improvements to the pavement structure are needed, and more expenditures are expected (medium rehabilitation). In addition, the structural capacity of the AC layer is adequate for most TSD routes. Only 0.19% (0.19%) of state routes have poor AC layers, but the current functional condition is good (fair). In this case, more pavement distress can be expected in the near future, and preventive maintenance is recommended for these sections.

Table 4-8. TSD routes assessment based on PMS

Route type		*Percentage*
Interstates	*Good PQI*	11.90%
	Fair PQI	85.72%
	Poor PQI	2.38%
State routes	*Good PQI*	35.07%
	Fair PQI	55.23%
	Poor PQI	9.70%

The current PMS focuses only on the pavement functional condition (**Table 4-8**) and fails to identify the underlying reasons for pavement deterioration. The value of the TSD lies in its ability to collect pavement structural information, which is not reliably or adequately captured by pavement performance indicators. The combination of PMS and DBPs (**Table 4-9**) allows for more appropriate decisions on maintenance and rehabilitation strategies and more accurate predictions of pavement conditions. It can be found that with the use of the PMS+DBPs system, the percentage of "Do nothing" route sections increases, while the percentage of monitored road sections decreases significantly. In addition, preliminary treatment recommendations are provided for those sections that need to be addressed. Therefore, the use of the PMS+DBPs system can reduce the investment in pavement management and enable more accurate allocations of funds.

Table 4-9. TSD routes assessment based on PMS+DBPs

Quality of Route Type		*Good & Fair AC*		*Poor AC*	
Route Type		*Good & Fair Subgrade*	*Poor Subgrade*	*Good & Fair Subgrade*	*Poor Subgrade*
Interstates	*Good PQI*	9.52%	2.38%	0	0
	Fair PQI	47.62%	38.10%	0	0
	Poor PQI	2.38%	0	0	0
State routes	*Good PQI*	31.15%	3.73%	0.19%	0
	Fair PQI	36.57%	18.47%	0.19%	0
	Poor PQI	2.05%	7.65%	0	0

Chapter 5 Conclusion

In this research project, a total of 959 miles of TSD data were collected throughout Tennessee. Approximately 80 miles of these TSD routes were overlapped to verify the repeatability of the TSD deflection data. FWD testing was conducted at 190 test sites, and FWD measurements were compared to the corresponding TSD measurements. The rank correlation analysis was also performed on TSD measurements and pavement performance data. In addition, the effect of load magnitude, test temperature, and test speed on TSD deflections were investigated, and practical guidelines for TSD data correction and analysis was provided to make the TSD deflection collected under different conditions comparable. A new approach to determine the effective SN with TSD measurements was developed by modifying the AASHTO method. Finally, the relationship between the TSD deflection lag and phase angle of the AC layer was investigated by 3D-Move simulations, and the possibility of estimating pavement conditions from TSD deflection lag was evaluated based on field TSD data. Based on the analyses presented, the following conclusions can be summarized:

1) TSD testing is time-efficient, and it is more suitable for network-level pavement evaluation than FWD.
2) The reliability and repeatability of raw TSD deflections was not fully verified from the current study. The TSD is recommended to be periodically validated by other devices, such as the FWD, for quality control.
3) The TSD deflection can be used to identify not only weak sections but also weak layers. The deflection indices D0, SCI_12, and D60 correspond to the strength of the entire pavement structure, AC layer, and subgrade, respectively. For example, the subgrade deformation (D60) in Region 4 is the highest, indicating that the subgrade in Region 4 is softer than other regions.
4) The effects of speed (loading time) and temperature on TSD deflections are equivalent, so the speed effect on pavement responses can be evaluated by the concept of "pseudo temperature."
5) TSD deflection is more sensitive to temperature than speed. At normal TSD driving speeds (20-60 mph), a 10 mph increase in speed is approximately equivalent to a 1°C drop in temperature.
6) The loading frequency of the TSD is lower than that of the FWD, and the AC layer exhibits lower stiffness under the TSD. Therefore, the TSD-based AASHTO SN is generally smaller than the FWD-based SN (error of 0.74). The TSD-based SN can be calibrated by AC thickness.
7) The lag distance increases with increasing fatigue levels until fatigue failure occurs. The lag distance is also related to pavement structures, temperature, and speed. For the same pavement structure, it is possible to identify the fatigued section by comparing the lag distance.
8) There is no significant correlation between TSD deflections and pavement performance. The value of the TSD lies in its ability to collect pavement structural information, which is not reliably or adequately captured by pavement performance indicators. The combination of pavement performance and the TSD (PMS+DBPs) allows for more

accurate prediction of pavement conditions and more appropriate decisions on maintenance and rehabilitation strategies.

Recommendations:

1) Due to the limited accuracy of the TSD, it cannot accurately measure deflections when pavement deformation is negligible. Therefore, it is recommended to increase the load magnitude of the TSD or to perform TSD testing during the warm season.
2) Periodic validation of the TSD by other devices such as FWD is recommended for quality control.
3) TSD deflections should be corrected to the same reference level before performing any analysis. The recommended procedure for TSD deflection correction is:

    Step 1: Determine the reference load magnitude, reference speed, and reference temperature. The recommended reference load magnitude, temperature, and speed are 82.2 psi, 20C, and 40 mph, respectively

    Step 2: Input the TSD deflections, load magnitude, test speed, and test temperature.

    Step 3: Input the thickness of the AC layer. (Optional: Input the AC dynamic modulus master curve function or ΔE_a).

    Step 4: Correct TSD deflections to the reference load magnitude.

    Step 5: Calculate the effective temperature based on test speed and test temperature using Equation (3-14).

    Step 6: Obtain the adjustment factor for the effective temperature based on AC thickness according to the AASHTO temperature correction method.

    Step 7: Apply the adjustment factor to the load-corrected D0 of the TSD to obtain the speed-and temperature-corrected D0.

4) It is recommended to collect additional and more representative TSD data to calibrate the thresholds of DBPs.

References

[1] S. W. Katicha, G. W. Flintsch, B. Ferne, and J. Bryce, “Limits of agreement method for comparing TSD and FWD measurements,” *Int. J. Pavement Eng.*, vol. 15, no. 6, pp. 532–541, Jul. 2014, doi: 10.1080/10298436.2013.782403.

[2] G. Flintsch, S. Katicha, J. Bryce, B. Ferne, S. Nell, and B. Diefenderfer, “Assessment of Continuous Pavement Deflection Measuring Technologies,” *SHRP 2 Rep.*, no. S2-R06F-RW-1, 2013, Accessed: Jul. 25, 2020. [Online]. Available: https://trid.trb.org/view/1244232

[3] M. Nasimifar, S. Thyagarajan, and N. Sivaneswaran, “Backcalculation of Flexible Pavement Layer Moduli from Traffic Speed Deflectometer Data,” *Transp. Res. Rec.*, vol. 2641, no. 1, pp. 66–74, Jan. 2017, doi: 10.3141/2641-09.

[4] B. W. Ferne, P. Langdale, N. Round, and R. Fairclough, “Development of a Calibration Procedure for the U.K. Highways Agency Traffic-Speed Deflectometer,” *Transp. Res. Rec. J. Transp. Res. Board*, vol. 2093, no. 1, pp. 111–117, Jan. 2009, doi: 10.3141/2093-13.

[5] W. B. Muller and J. Roberts, “Revised approach to assessing traffic speed deflectometer data and field validation of deflection bowl predictions,” *Int. J. Pavement Eng.*, vol. 14, no. 4, pp. 388–402, Apr. 2013, doi: 10.1080/10298436.2012.715646.

[6] A. Zofka, J. Sudyka, M. Maliszewski, P. Harasim, and D. Sybilski, “Alternative Approach for Interpreting Traffic Speed Deflectometer Results,” *Transp. Res. Rec.*, vol. 2457, no. 1, pp. 12–18, Jan. 2014, doi: 10.3141/2457-02.

[7] G. Chai, S. Manoharan, A. Golding, G. Kelly, and S. Chowdhury, “Evaluation of the Traffic Speed Deflectometer Data Using Simplified Deflection Model,” *Transp. Res. Procedia*, vol. 14, pp. 3031–3039, Jan. 2016, doi: 10.1016/j.trpro.2016.05.444.

[8] R. Wix, C. Murnane, and M. Moffatt, “Experience Gained Investigating, Acquiring and Operating the First Traffic Speed Deflectometer in Australia,” *Transp. Res. Procedia*, vol. 14, pp. 3060–3069, Jan. 2016, doi: 10.1016/j.trpro.2016.05.450.

[9] Diefenderfer, Brian K, "Investigation of the rolling wheel deflectometer as a network-level pavement structural evaluation tool." No. VTRC 10-R5; FHWA/VTRC 10-R5. Virginia Transportation Research Council, 2010.

[10] Rada, Gonzalo R., Soheil Nazarian, Beth A. Visintine, Raj V. Siddharthan, and Senthil Thyagarajan. "Pavement structural evaluation at the network level. No. FHWA-HRT-15-074. United States," Federal Highway Administration. Office of Infrastructure Research and Development, 2016.

[11] M. A. Elseifi, Z. U. A. Zihan, and Louisiana Transportation Research Center, “Assessment of the Traffic Speed Deflectometer in Louisiana for Pavement Structural Evaluation,” FHWA/LA.18/590, Mar. 2018. Accessed: Feb. 21, 2022. [Online]. Available: https://rosap.ntl.bts.gov/view/dot/36793

[12] M. Zhang *et al.*, “Numerical investigation of pavement responses under TSD and FWD loading,” *Constr. Build. Mater.*, vol. 318, p. 126014, Feb. 2022, doi: 10.1016/j.conbuildmat.2021.126014.

[13] C. Wu, H. Wang, J. Zhao, X. Jiang, and Y. Qiu, “Asphalt pavement modulus backcalculation using surface deflections under moving loads,” *Comput.-Aided Civ. Infrastruct. Eng.*, vol. 35, no. 11, pp. 1246–1260, 2020, doi: 10.1111/mice.12624.

[14] M. Y. Kim, D. Y. Kim, and M. R. Murphy, “Improved Method for Evaluating the Pavement Structural Number with Falling Weight Deflectometer Deflections,” *Transp. Res. Rec.*, vol. 2366, no. 1, pp. 120–126, Jan. 2013, doi: 10.3141/2366-14.
[15] Rohde, Gustav T. "Determining pavement structural number from FWD testing." *Transportation Research Record 1448* (1994).
[16] Transportation Officials. AASHTO Guide for Design of Pavement Structures, 1993. Vol. 1. Aashto, 1993.
[17] S. Alavi, J. F. LeCates, and M. P. Tavares, “Falling Weight Deflectometer Usage,” *NCHRP Synth. Highw. Pract.*, no. 381, 2008, Accessed: Jul. 24, 2020. [Online]. Available: https://trid.trb.org/view/871781
[18] K. Maser, P. Schmalzer, W. Shaw, and A. Carmichael, “Integration of Traffic Speed Deflectometer and Ground-Penetrating Radar for Network-Level Roadway Structure Evaluation,” *Transp. Res. Rec.*, vol. 2639, no. 1, pp. 55–63, Jan. 2017, doi: 10.3141/2639-08.
[19] Z. Uddin Ahmed Zihan, M. A. Elseifi, K. Gaspard, and Z. Zhang, “Development of a Structural Capacity Prediction Model Based on Traffic Speed Deflectometer Measurements,” *Transp. Res. Rec.*, vol. 2672, no. 40, pp. 315–325, Dec. 2018, doi: 10.1177/0361198118758058.
[20] M. Nasimifar, S. Thyagarajan, S. Chaudhari, and N. Sivaneswaran, “Pavement Structural Capacity from Traffic Speed Deflectometer for Network Level Pavement Management System Application,” *Transp. Res. Rec.*, vol. 2673, no. 2, pp. 456–465, Feb. 2019, doi: 10.1177/0361198118825122.
[21] Flintsch, G. W., B. Ferne, B. Diefenderfer, S. Katicha, J. Bryce, and S. Nell. "Valuation of traffic speed continuous deflection devices." In 91st Annual Meeting, Transport Research Board, USA. 2012.
[22] Rada, Gonzalo R., Soheil Nazarian, Beth A. Visintine, Raj V. Siddharthan, and Senthil Thyagarajan. Pavement structural evaluation at the network level. No. FHWA-HRT-15-074. United States. Federal Highway Administration. Office of Infrastructure Research and Development, 2016.
[23] Y. Deng, X. Luo, F. Gu, Y. Zhang, and R. L. Lytton, “3D simulation of deflection basin of pavements under high-speed moving loads,” *Constr. Build. Mater.*, vol. 226, pp. 868–878, Nov. 2019, doi: 10.1016/j.conbuildmat.2019.07.228.
[24] Elseifi, Mostafa A., Zia UA Zihan, and Patrick Icenogle. "A Mechanistic Approach to Utilize Traffic Speed Deflectometer (TSD) Measurements into Backcalculation Analysis." No. FHWA/LA. 17/612. Louisiana State University. Department of Civil and Environmental Engieering, 2019.
[25] R. V. Siddharthan, J. Yao, and P. E. Sebaaly, “Pavement Strain from Moving Dynamic 3D Load Distribution,” *J. Transp. Eng.*, vol. 124, no. 6, pp. 557–566, Nov. 1998, doi: 10.1061/(ASCE)0733-947X (1998)124:6(557).
[26] S. T. Dai, D. Van Deusen, M. Beer, D. Rettner, and G. Cochran, “INVESTIGATION OF FLEXIBLE PAVEMENT RESPONSE TO TRUCK SPEED AND FWD LOAD THROUGH INSTRUMENTED PAVEMENTS,” presented at the Eighth International Conference on Asphalt PavementsFederal Highway Administration, 1997. Accessed: Apr. 21, 2021. [Online]. Available: https://trid.trb.org/view/501627
[27] Nielsen, Christoffer P. "Visco-elastic back-calculation of traffic speed deflectometer measurements." Transportation research record 2673, no. 12 (2019): 439-448.

[28] Lytton, Robert L., *Determining Asphaltic Concrete Pavement Structural Properties by Nondestructive Testing*. Transportation Research Board, 1990.
[29] I. L. Al-Qadi, W. Xie, and M. Elseifi, "Frequency determination from vehicular loading time pulse to predict appropriate complex modulus in MEPDG," *Asph. Paving Technol. Assoc. Asph. Paving Technol.-Proc. Tech. Sess.*, vol. 77, pp. 739–771, Jan. 2008.
[30] ARA (Applied Research Associates), "Guide for mechanistic- empirical design of new and rehabilitated pavement structures," Washington, DC: Transportation Research Board of the National Academies., Final Report No. NCHRP 1-37A, 2004.
[31] Fu, Guozhi, Yanqing Zhao, Changjun Zhou, and Wanqiu Liu. "Determination of effective frequency range excited by falling weight deflectometer loading history for asphalt pavement." Construction and Building Materials 235 (2020): 117792.
[32] V. P. Le, H. J. Lee, J. M. Flores, W. J. Kim, and J. Baek, "New Approach to Construct Master Curve of Damaged Asphalt Concrete Based on Falling Weight Deflectometer Back-Calculated Moduli," *J. Transp. Eng.*, vol. 142, no. 11, p. 04016048, Nov. 2016, doi: 10.1061/(ASCE)TE.1943-5436.0000881.
[33] R. V. Siddharthan, N. Krishnamenon, and P. E. Sebaaly, "Finite-Layer Approach to Pavement Response Evaluation," *Transp. Res. Rec.*, vol. 1709, no. 1, pp. 43–49, Jan. 2000, doi: 10.3141/1709-06.
[34] R. V. Siddharthan, N. Krishnamenon, M. El-Mously, and P. E. Sebaaly, "Validation of a Pavement Response Model Using Full-scale Field Tests," *Int. J. Pavement Eng.*, vol. 3, no. 2, pp. 85–93, Jan. 2002, doi: 10.1080/10298430290030595.
[35] A. Ulloa, E. Y. Hajj, R. V. Siddharthan, and P. E. Sebaaly, "Equivalent Loading Frequencies for Dynamic Analysis of Asphalt Pavements," *J. Mater. Civ. Eng.*, vol. 25, no. 9, pp. 1162–1170, Sep. 2013, doi: 10.1061/(ASCE)MT.1943-5533.0000662.
[36] T. K. Pellinen, M. W. Witczak, and R. F. Bonaquist, "Asphalt Mix Master Curve Construction Using Sigmoidal Fitting Function with Non-Linear Least Squares Optimization," pp. 83–101, Apr. 2004, doi: 10.1061/40709(257)6.
[37] Akima, Hiroshi. "A method of bivariate interpolation and smooth surface fitting based on local procedures." Communications of the ACM 17, no. 1 (1974): 18-20.
[38] B. Huang, X. Shu, and J. Bass, "Investigation of Simple Performance Characteristics of Plant-Produced Asphalt Mixtures in Tennessee," *Transp. Res. Rec.*, vol. 2057, no. 1, pp. 140–148, Jan. 2008, doi: 10.3141/2057-17.
[39] Breiman, Leo, Jerome H. Friedman, Richard A. Olshen, and Charles J. Stone. Classification and regression trees. Routledge, 2017.
[40] Y. Wang, Mahboub Kamyar C., and Hancher Donn E., "Survival Analysis of Fatigue Cracking for Flexible Pavements Based on Long-Term Pavement Performance Data," *J. Transp. Eng.*, vol. 131, no. 8, pp. 608–616, Aug. 2005, doi: 10.1061/(ASCE)0733-947X(2005)131:8(608).
[41] Grogg, M., Van, T., Rozycki, R., Vaughn, R., Roff, T., Clarke, J., ... & Chang, C. (2018). FHWA Computation Procedure for the Pavement Condition Measures (No. FHWA-HIF-18-022). United States. Federal Highway Administration.
[42] M. A. Elseifi, K. Gaspard, P. W. Wilke, Z. Zhang, and A. Hegab, "Evaluation and Validation of a Model for Predicting Pavement Structural Number with Rolling Wheel Deflectometer Data," *Transp. Res. Rec.*, vol. 2525, no. 1, pp. 13–19, Jan. 2015, doi: 10.3141/2525-02.
[43] C. Chang *et al.*, "TXDOT guidelines to assign PMIS treatment levels.," 0-6673-P1, Jun. 2014. Accessed: Feb. 21, 2022. [Online]. Available: https://rosap.ntl.bts.gov/view/dot/27746

Appendices

Appendix A: DOT Survey Summary

Through an online survey of the State and Provincial Departments of Transportation (DOTs), the demand and potential value of continuous deflectometer such as TSD was evaluated. The survey focused on assessing the main concerns in applying continuous deflectometers and the primary uses of network-level deflection data.

The online survey received responses from 29 states. Almost all states have their own network-level PMS, but 58.6% of states make M&R strategy decisions based on their PMS. Only 24.1% of states include pavement structural capacity information in their PMS, while 17.2% of states include deflection information. 89.7% of state agencies believe that deflection best reflects the structural capacity of a pavement, but there is significant disagreement about which deflection index is more valuable. More than 93% of states currently conduct FWD testing, and only 37.9% of states have tried TSD. 75.9% of states have complaints about traffic control during FWD testing, but the main issues with applying continuous deflectometers like TSD for network-level data collection are the cost of TSD testing and how to incorporate TSD deflection data into the PMS. About 70% of states desire to collect network-level data to improve PMS and identify strong and weak sections. The main application of deflection data is to perform back-calculation of layer modulus. The following are the details of the survey:

1. Does your state have a network-level pavement management system (PMS)?

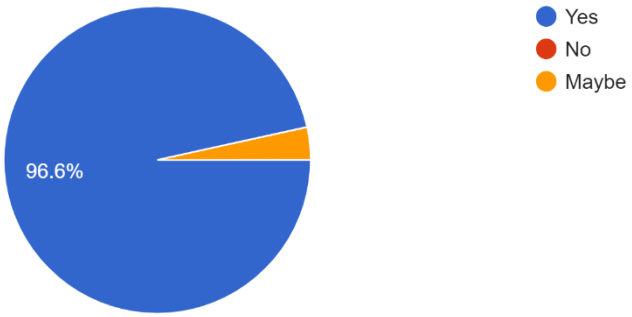

2. Does your state make maintenance and rehabilitation strategy decisions based on PMS?

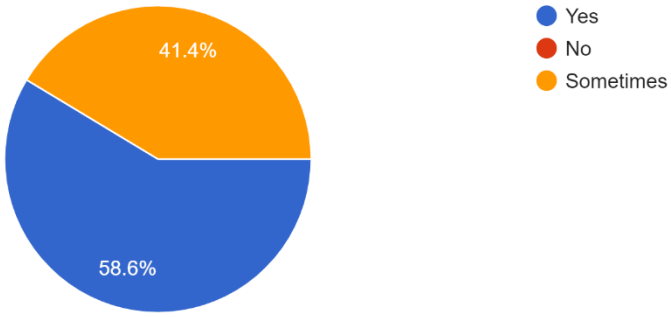

3. Does the PMS in your state contain pavement strength information (e.g., structure number)?

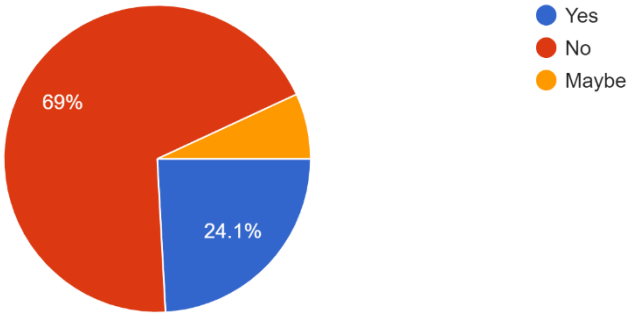

4. Does the PMS in your state incorporate deflection information?

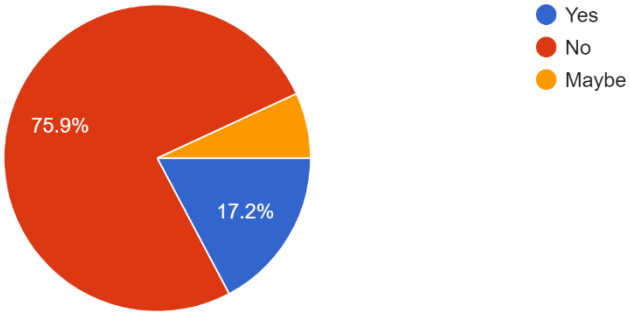

5. Do you think the pavement performance is directly related to pavement structural capacity?

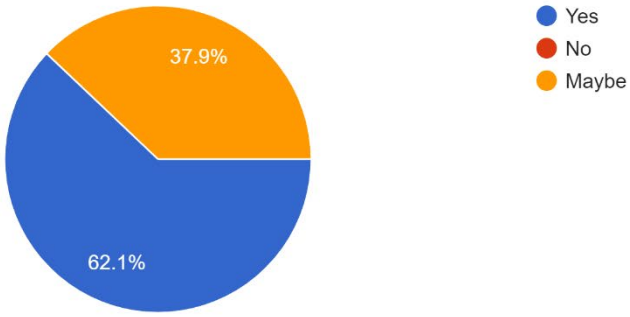

6. Which indicators do you think best reflect pavement structural capacity? (Multiple choices)

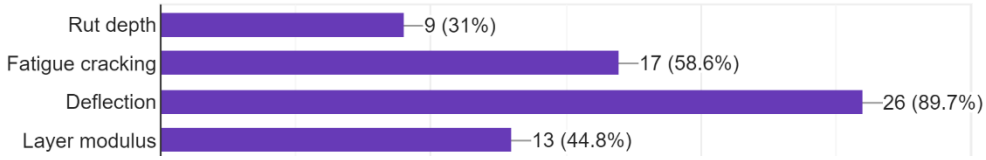

Except for the above options, some agencies also recommend the structure number and layer thickness to indicate pavement structural capacity. In addition, some agencies believe that deflection and layer modulus can help determine structural adequacy, but specific values may not be recommended. For example, a pavement structure is considered good for a two-lane highway with 250 trucks per day but may not necessarily be adequate for very high traffic volumes. Therefore, the presence of pavement distress is more indicative of the poor structural capacity of the pavement.

7. Which deflection test output do you think is more valuable? (Multiple choices)

8. How does your state use deflection test results? (Multiple choices)

Except for the above options, some agencies mention load transfer testing and void detection using deflection results. In addition, many agencies use the deflection results to back-calculate the modulus or strain and then calculate the required overlay thickness by meeting structural number or strain requirements.

9. Does your state typically verify the layer thickness (e.g., core samples, ground-penetrating radar) before performing the layer modulus back-calculation?

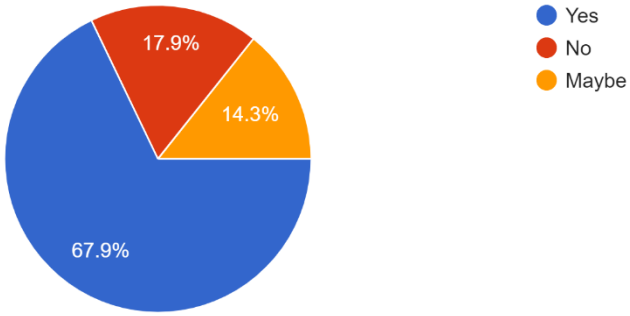

10. Which equipment is used for pavement deflection tests in your state? (Multiple choices)

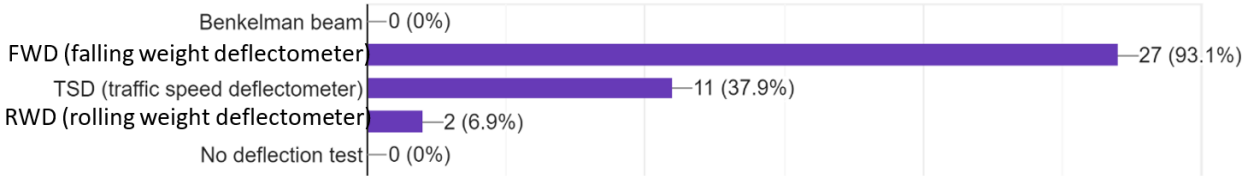

11. What do you think are the main disadvantages of FWD tests? (Multiple choices)

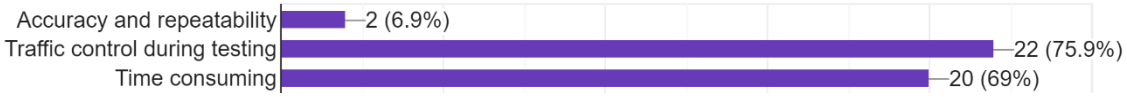

12. Does your state prefer TSD over traditional deflection tests for speed efficiency?

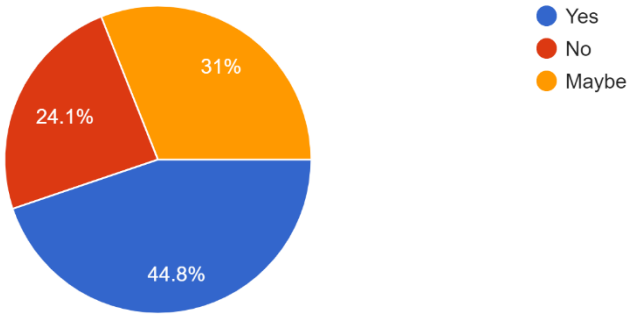

13. What are the main concerns for your state to use a continuous deflectometer like TSD? (Multiple choices)

In addition to the above options, some agencies have expressed concern about the infrequent use of deflection in pavement design.

14. Is your state interested in network-level pavement assessment based on deflection?

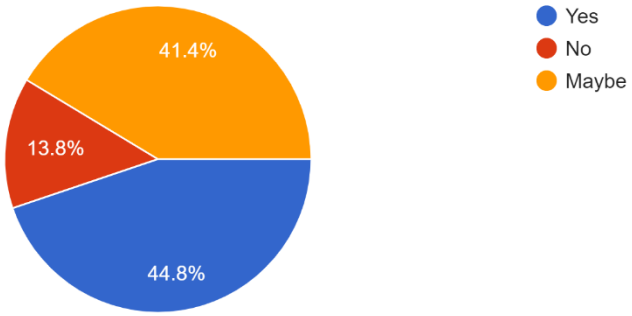

15. What does your state most want to do with network-level deflection data? (Multiple choices)

Some organizations complain about the cost of TSD testing and feel reluctant to use it unless the cost drops significantly.

16. What key engineering parameters does your state wish to derive from the deflection test? (Multiple choices)

Appendix B: Additional Figures

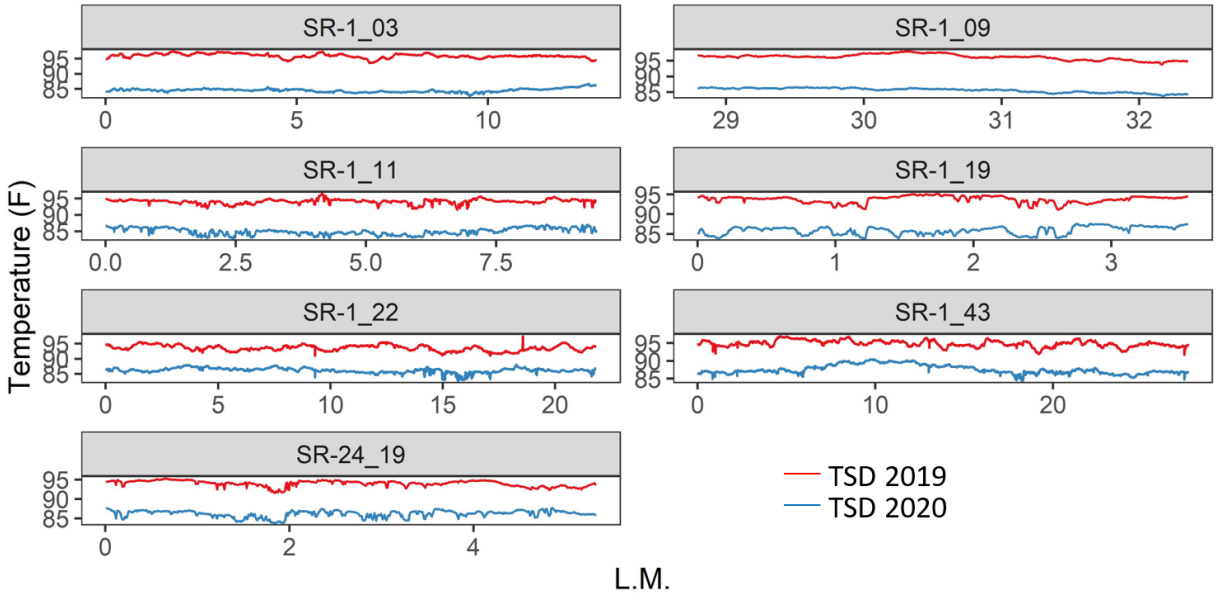

Figure A-1. **Temperature comparison for overlapping TSD routes**

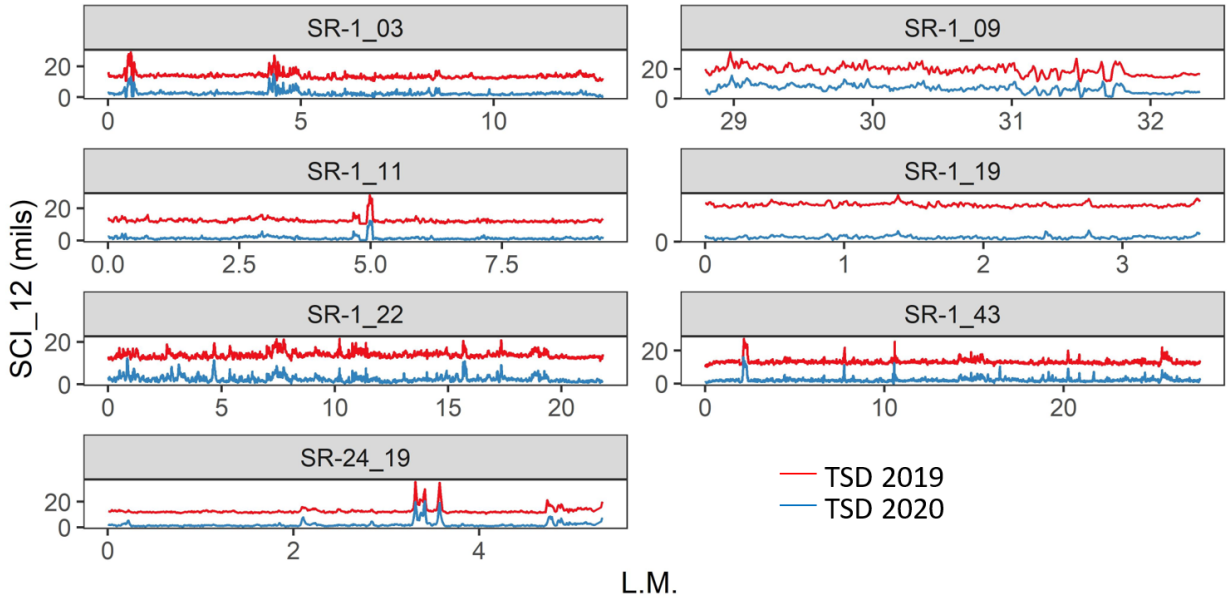

Figure A-2. **SCI_12 comparison for overlapping TSD routes**

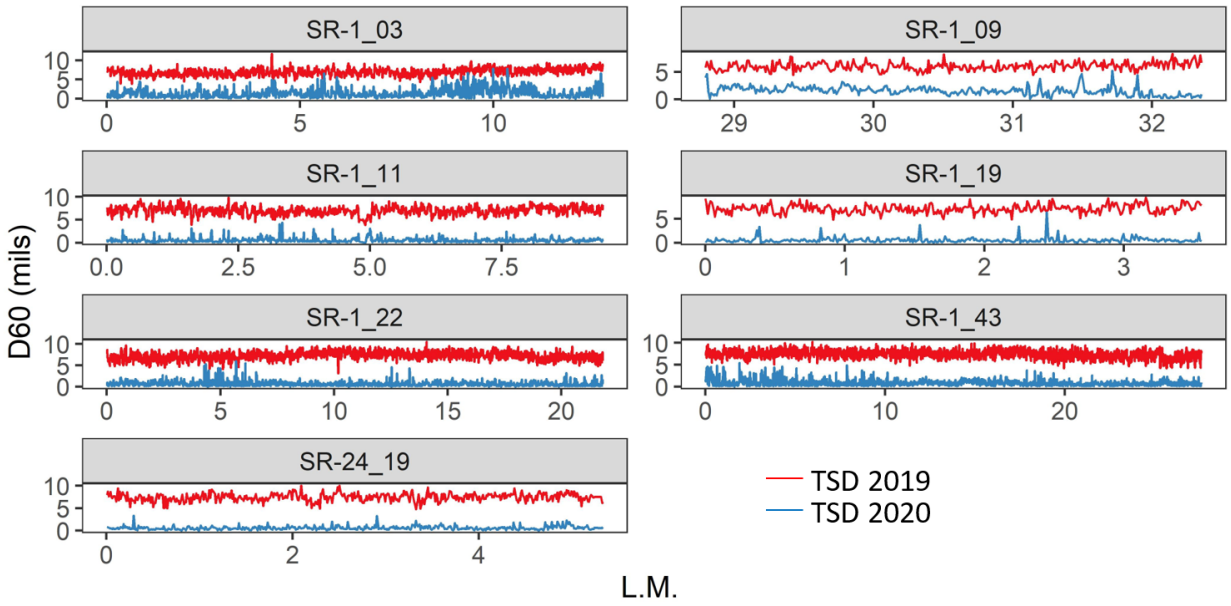

Figure A-3. **D60 comparison for overlapping TSD routes**

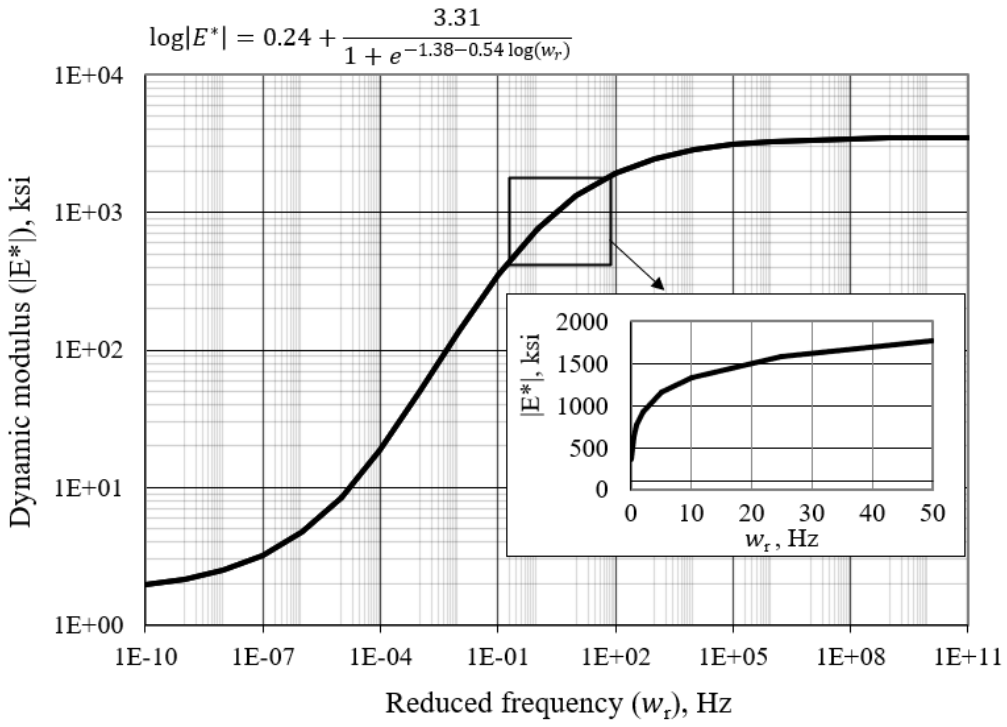

Figure A-4. **Dynamic modulus of the AC layer at 68 °F**

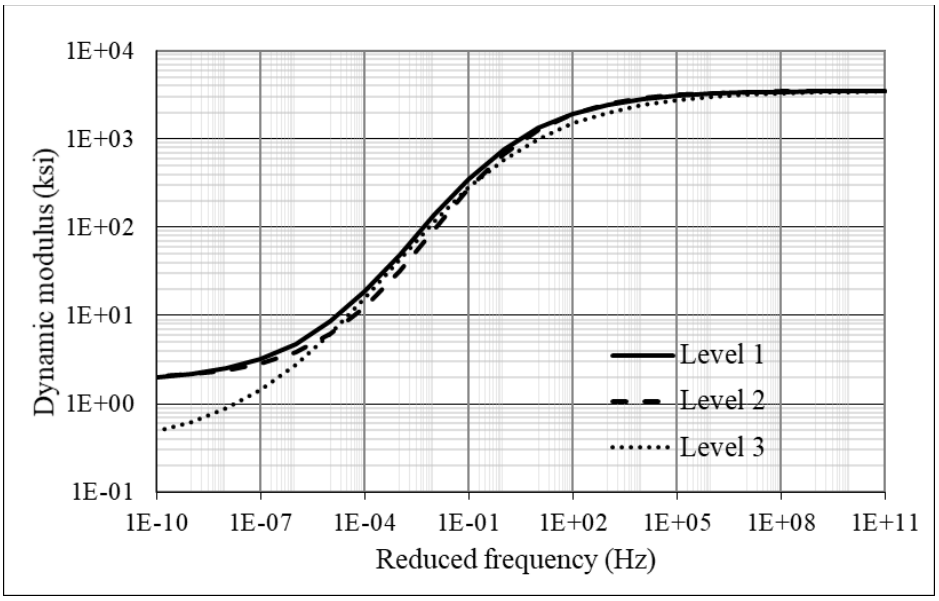

Figure A-5. **The dynamic modulus curves of three plant-produced AC materials at 68 °F**

Index Parameters	Asphalt Thickness, in.				Diagnosis
	>5	<=5,>=2.5	<2.5,>=1	<1	
SCI	<4	<6	<12	<16	Very Good Asphalt Layer
	4-6	6-10	12-18	16-24	Good Asphalt Layer
	6-8	10-15	18-24	24-32	Fair Asphalt Layer
	8-10	15-20	24-30	32-40	Poor Asphalt Layer
	>10	>20	>30	>40	Very Poor Asphalt Layer
BCI	<2	<3	<4	<8	Very Good Base Layer
	2-3	3-5	4-8	8-12	Good Base Layer
	3-4	5-9	8-12	12-16	Fair Base Layer
	4-5	8-10	12-16	16-20	Poor Base Layer
	>5	>10	>16	>20	Very Poor Base Layer
w7	<1	<1	<1	<1	Very Good Subgrade Layer
	1-1.4	1-1.4	1-1.4	1-1.4	Good Subgrade Layer
	>1.4-1.8	>1.4-1.8	>1.4-1.8	>1.4-1.8	Fair Subgrade Layer
	>1.8-2.2	>1.8-2.2	>1.8-2.2	>1.8-2.2	Poor Subgrade Layer
	>2.2	>2.2	>2.2	>2.2	Very Poor Subgrade Layer

Figure A-6. **Structural condition assessment in Texas [43]**